ARTICLE

doi:10.1038/nature17144

A hippocampal network for spatial coding during immobility and sleep

Kenneth Kay[1], Marielena Sosa[1], Jason E. Chung[1], Mattias P. Karlsson[1], Margaret C. Larkin[1] & Loren M. Frank[1,2]

How does an animal know where it is when it stops moving? Hippocampal place cells fire at discrete locations as subjects traverse space, thereby providing an explicit neural code for current location during locomotion. In contrast, during awake immobility, the hippocampus is thought to be dominated by neural firing representing past and possible future experience. The question of whether and how the hippocampus constructs a representation of current location in the absence of locomotion has been unresolved. Here we report that a distinct population of hippocampal neurons, located in the CA2 subregion, signals current location during immobility, and does so in association with a previously unidentified hippocampus-wide network pattern. In addition, signalling of location persists into brief periods of desynchronization prevalent in slow-wave sleep. The hippocampus thus generates a distinct representation of current location during immobility, pointing to mnemonic processing specific to experience occurring in the absence of locomotion.

The hippocampus is essential for memory and spatial navigation, but we still do not know how these cognitive functions are made possible by the hippocampal neural circuit. Examination of hippocampal neural activity during naturalistic behaviours yields a landmark clue: during locomotion, hippocampal principal neurons, known as 'place' cells, fire when subjects traverse discrete locations in space[1,2]. Place cell firing thus provides an internal representation of space understood to be required for both spatial navigation and episodic memory[1,3,4]. Yet despite extensive study of place cells, it remains an open question whether place firing reliably persists in the absence of movement, and, if so, whether distinct hippocampal neurons and network mechanisms are engaged. This matter is of fundamental importance as immobility punctuates spatial exploration[5,6] and features in a range of behaviours dependent on the hippocampus[1,7,8], including contextual fear conditioning[9] and trace conditioning[10].

Previous work focusing on hippocampal neural activity during immobility has identified firing related to past and even upcoming experience[11–15]. Most striking is the observation that place cells during immobility often re-activate in brief bouts at locations outside of their spatial receptive fields. These brief re-activations occur in conjunction with hippocampal sharp wave-ripples (SWRs)[16,17], massively synchronous network events lasting ~100 ms and reflecting high firing rates and strong excitatory drive in hippocampal subregions CA1, CA3, and DG[1,16–20]. Recent work indicates that place cell firing during SWRs frequently represents spatial sequences remote from the animal's current position[14,17,21–23], further raising the question of whether and how the hippocampus sustains a representation of current position during immobility.

A distinct neuron population at CA2

We recorded neural activity in hippocampal subregions CA1, CA2, CA3, and DG (Fig. 1a) in rats engaged in a hippocampus-dependent spatial memory task[21,24], with interleaved rest sessions in an enclosed box. In the task, subjects were trained to alternate between each of three locations (reward wells) in a W-shaped maze (Extended Data Fig. 1a). In examining single neuron (unit) activity, we observed principal units (Fig. 1b) that fired at continuously high rates during immobility (Extended Data Fig. 2a). This basic observation led us to investigate hippocampal activity in this behavioural state.

We first found that, although SWRs were prominent during immobility, SWR periods comprised only a small proportion of time spent immobile (<10%, Extended Data Fig. 2b), suggesting that SWRs could not account for the observed continuous firing. Next, in examining unit firing at the time of SWRs, we were struck by putative principal units recorded in CA2 that consistently decreased firing during both task and rest SWRs, in contrast to CA1 and CA3 principal units, which increased firing (Fig. 1c, d). Indeed virtually all CA1 and CA3 principal units fired more during SWRs (permutation tests at $P < 0.05$, CA1: 478 out of 489 units, CA3: 271 out of 276 units), while a substantial proportion of putative principal units recorded at CA2 sites were either inhibited or showed no change in firing rate during SWRs, despite otherwise firing hundreds to thousands of spikes during single task epochs (84 out of 226 CA2 site units, with 56 of 84 significantly inhibited during SWRs; Fig. 1e and Extended Data Fig. 3). We termed these atypical units at CA2 sites 'N' units (non-positively modulated by SWRs) to distinguish them from conventionally responding 'P' units (positively modulated).

N units fire more during immobility

We next examined the relationship of N unit firing to ongoing behaviour. We found that N units fired mainly at low movement speeds and during immobility (Fig. 2a). To characterize this relationship, we first evaluated the correlation between unit firing rate and speed (Fig. 2b). The CA1 and CA3 unit populations both showed overall positive correlation, consistent with previous reports[25–27] (Pearson's r, firing rate versus log speed; mean ± s.d.; CA1: 0.11 ± 0.10, CA1 versus 0, $P < 10^{-58}$, signed-rank; CA3: 0.06 ± 0.11, CA3 versus 0, $P < 10^{-14}$, signed-rank). Remarkably, the CA2 N and CA2 P unit populations showed dramatically different distributions: P units were positively correlated while N units were almost exclusively negatively correlated (mean ± s.d.; CA2 P: 0.10 ± 0.13, CA2 P versus 0, $P < 10^{-11}$, signed-rank; CA2 N: -0.10 ± 0.09, CA2 N versus 0, $P < 10^{-10}$, signed-rank; CA2 N versus CA2 P, $P < 10^{-19}$, rank-sum). N units also fired at higher rates than all other unit populations during immobility (Fig. 2c). These findings indicated a fundamental distinction between N units and classic hippocampal place cells.

[1]UCSF Center for Integrative Neuroscience and Department of Physiology, University of California San Francisco, California 94158, USA. [2]Howard Hughes Medical Institute, University of California San Francisco, California 94158, USA.

© 2016 Macmillan Publishers Limited. All rights reserved

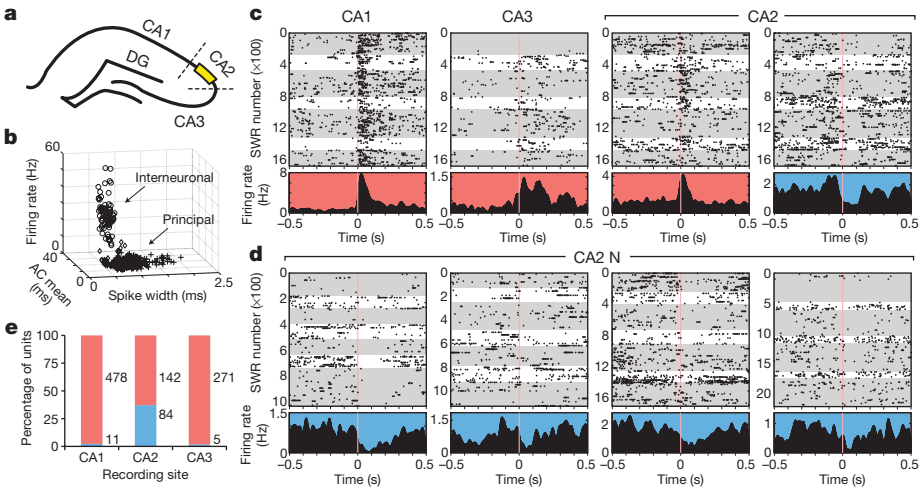


Figure 1 | Distinct hippocampal neuron population at CA2.
a, Diagram of hippocampal recording sites. Recording locations were designated as CA2 sites if found to overlap with the CA2 cytoarchitectural locus[50]. A molecularly defined CA2 region is shown as a yellow band. Additional description is provided in Extended Data Fig. 1.
b, Classification of putative principal versus interneuronal units. Shown is a scatter plot of all hippocampal neural units in the task data set for the three features used to classify units in this study. AC mean: autocorrelation function mean. Open circles: interneuronal ($n = 78$); plus symbols: principal ($n = 991$); open diamonds: unclassified ($n = 21$). **c**, Firing aligned to SWRs ($t = 0$: time of SWR onset) in four simultaneously recorded hippocampal putative principal units. Upper sections: SWR-triggered spike rasters (black dots). Grey zones demarcate rest epochs; white zones demarcate task epochs. Lower sections: peri-SWR time histogram (PSTH; 1-ms bins) smoothed with a Gaussian kernel ($\sigma = 10$ ms). Red background indicates increased firing during SWRs; blue background indicates lack of increase. The CA2 site units were recorded on the same tetrode. **d**, Firing aligned to SWRs in four example CA2 N units. Each unit was recorded from a different subject. **e**, Percentages of P (red) versus N (blue) units at CA1, CA2, and CA3 recording sites. Numbers correspond to unit counts.

N units signal location during immobility

We next assessed whether N units showed spatial firing. We found that N units showed less spatial coverage than the other unit populations (Fig. 3a, b and Extended Data Fig. 4). In contrast, CA2 P units typically showed large spatial fields, consistent with recent reports[28–30].

In conjunction with low spatial coverage, N unit firing maps showed concentrated firing at locations where subjects were immobile (Fig. 3a and Extended Data Fig. 4c). To quantify possible spatial specificity in firing during immobility, we focused on firing at the maze reward wells since immobility at these locations was common across all subjects. Our analysis revealed that individual N units characteristically fired at specific single reward wells, while remaining silent at the others (Fig. 3c, d and Extended Data Fig. 5a). The location of N unit firing did not require direct association with reward since spatially specific firing was also observed at other maze locations

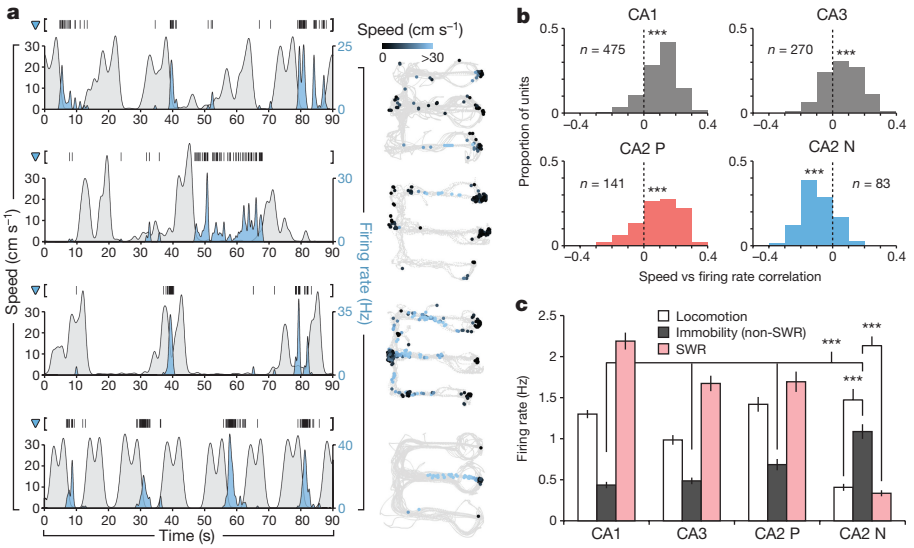


Figure 2 | N units fire more at low speeds and during immobility.
a, Firing of four example CA2 N units during task behaviour. Each row corresponds to an N unit, with spike rasters plotted above the traces. Left y axis and grey fill trace: head speed (cm s^{-1}) of the subject. Right y axis and blue fill trace: instantaneous firing rate (Hz). Right panels: spatial firing maps from corresponding task epochs. Grey: positions visited; coloured points (darker colour values at lower speeds): positions at which firing occurred, with each point opaque and plotted chronologically.
b, Distribution of correlations (Pearson's r) between firing rate and log speed for each hippocampal unit population. ***$P < 0.001$ (versus $r = 0$).
c, Mean firing rates during task epochs (mean ± s.e.m.; number of units: CA1: 478, CA3: 271, CA2 P: 142, CA2 N: 84). Across unit populations, N units showed the highest firing rates during non-SWR immobility (Kruskal–Wallis ANOVA, Tukey's post hoc tests for CA2 N greater than each other population, $P < 0.001$). Moreover, N unit firing was higher during non-SWR immobility than during locomotion ($P < 10^{-10}$, signed-rank) and also SWRs ($P < 10^{-12}$, signed-rank). ***$P < 0.001$.

© 2016 Macmillan Publishers Limited. All rights reserved

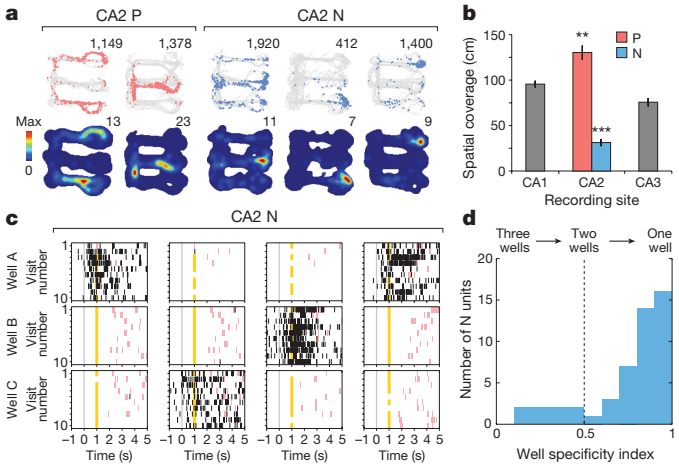


Figure 3 | N units signal current location during immobility. a, Spatial firing maps of five example CA2 site units. Each column corresponds to a unit. Upper row: positions visited (grey) and positions where the unit fired (coloured points: P units in red, N units in blue). Total number of spikes is reported at upper right. Lower row: occupancy-normalized firing maps. Peak spatial firing rate is reported at upper right. Subjects stopped locomoting at the ends of the maze arms to receive reward and also stopped intermittently elsewhere in the maze (Extended Data Fig. 1a). **b**, Spatial coverage in the hippocampal unit populations (mean ± s.e.m.; number of units: CA1: 476, CA2 P: 142, CA2 N: 79, CA3: 271). The CA2 N and P unit populations showed the lowest and highest spatial coverages, respectively (Kruskal–Wallis ANOVA, Tukey's post hoc tests, CA2 P greater than each other population, $P = 0.0015$; CA2 N less than each other population, $P < 10^{-6}$). $^{**}P < 0.01$; $^{***}P < 0.001$. **c**, Reward well firing of four example CA2 N units. Each column corresponds to a unit. For each well, the last ten visits (in a task recording epoch) are shown. Grey line: time of well entry ($t = 0$); yellow line: time of reward delivery (omitted in error trials). SWR periods are shown as pink zones. The two leftmost units were recorded simultaneously and on the same tetrode. **d**, Well specificity distribution in the N unit population. Mean ± s.e.m.: 0.78 ± 0.03 ($n = 53$ units).

(Extended Data Fig. 5b–d; seen previously in Fig. 2a and Extended Data Fig. 4c). These findings indicate that N unit firing constitutes a precise neural code for location during immobility.

A signature of spatial coding during immobility

We were struck by the fact that the firing pattern of N units not only was unorthodox (Fig. 1), but also had unambiguous behavioural (Fig. 2) and representational (Fig. 3) correlates. We hypothesized that this distinctive firing was the result of an unidentified input pattern in the hippocampus. To evaluate this possibility, we calculated CA2 site (N and P) unit spike-triggered averages (STAs) of hippocampal local field potential (LFP)[18], analysing locomotor and immobility periods separately (Fig. 4a).

In contrast to STAs from locomotor periods (characterized by the expected ~8 Hz theta frequency modulation[18,31], Extended Data Fig. 6), STAs from non-SWR immobility periods (Fig. 4b, c and Extended Data Fig. 7a) showed that N units fired at the time of a positive transient LFP pattern lasting ~200 ms. The pattern was smallest on the parent electrode in CA2, larger in CA3, and largest at DG, suggesting broad engagement of the hippocampal circuit. Furthermore, unlike N units, P units showed a mean STA characterized by a negative transient similar to the canonical sharp wave transient of SWRs[32] (Fig. 4b, c).

Power spectral analysis (Fig. 4d) further specified the contrasting LFP patterns. The power spectral density (PSD) of CA2 N and P unit immobility STAs and of SWR sharp waves showed fundamental frequencies <5 Hz, a bandwidth distinct to that of theta[18,31] (5–11 Hz). In agreement, STAs of LFP filtered at 1–4 Hz showed the same pattern of transients as in the wide-band STAs (Extended Data Fig. 7a), indicating that filtering at 1–4 Hz effectively isolates the large-amplitude transients associated with CA2 N units, CA2 P units, and SWRs. The N unit STA pattern exceeded 0 mV (Extended Data Fig. 7b, c), in fundamental contrast to SWR sharp waves[32], which manifested as negative transients. Thus, N units fired in association with an LFP pattern distinct from canonical hippocampal LFP patterns[1,17,18] (theta and SWRs). We termed this pattern 'N wave' (N unit-identified wave), a ~200 ms LFP transient with positive polarity at hippocampal recording sites (specifically CA2, CA3, and DG principal cell layers) at which SWR sharp waves are negative.

We then asked whether neurons outside of CA2 were also N wave-coupled. We identified N wave-coupled units in CA1, CA3, and DG (Fig. 4e–i and Extended Data Figs 7d-g, 8, 9), indicating that the N wave reflects a hippocampus-wide network pattern. Critically, a distinct subset of principal units was N-wave coupled (CA1: 50 units, CA3: 34 units, Fig. 4g–i and Extended Data Figs 8 and 9). As with CA2 N units, these units fired more during immobility than during movement (Extended Data Fig. 8b) and showed unequivocal location-specific firing during immobility (Fig. 4g, i and Extended Data Figs 8d, e and 9), thereby linking the N wave network pattern to spatial coding during immobility across the hippocampus.

Hippocampal spatial coding in sleep

Does spatial coding during immobility also occur under quiescent behavioural conditions? Intriguingly, past work has shown that, during slow-wave sleep, ~5% of CA1 place cells continuously fire during episodes in which hippocampal neural activity becomes highly desynchronized, reflected by low-amplitude LFP[33]. In this sleep state, termed small-irregular activity (SIA)[1,33,34], CA1 place cells were found to signal the location where the subject fell asleep (nesting position)[33]. Recent findings show that CA2 neurons send strong excitatory input to CA1 (refs 35–37), raising the possibility that coding of nesting position is staged upstream in CA2.

To test this possibility, we evaluated hippocampal neural activity during rest sessions. First, during sleep, we observed periods of high-amplitude LFP, corresponding to a hippocampal sleep state dominated by SWRs (termed LIA[1,18,33,34]), frequently interrupted by periods of low-amplitude LFP in which the subject did not rouse, which we identified as periods of SIA (Fig. 5a). Next, in examining unit firing during sleep, we observed striking instances in which N units fired preferentially during SIA periods, falling silent during LIA (Fig. 5b). Analogously to awake immobility in the task (Fig. 2c), the N unit population fired at higher rates than all other unit populations during SIA (green, Fig. 5c) and also during awake immobility in the rest environment (dark grey, Fig. 5c). However, unlike the task condition, there was no significant overall correlation between firing rate and speed for N units during awake periods in the rest environment (Extended Data Fig. 10a), indicating that properties of the task maze or the cognitive demands of the task have essential roles in regulating N unit firing.

We then asked whether N units represented locations in the rest environment. We found that N units showed spatially specific firing during awake periods (Fig. 5d, Extended Data Fig. 10b) that persisted in awake immobility periods (Extended Data Fig. 10c–i) and furthermore into SIA: specifically, the CA1 and N unit populations met dual criteria for nesting position coding during SIA, while the CA3 population unexpectedly failed both criteria (criteria in Supplementary Methods; Fig. 5e, f and Extended Data Fig. 10j–l). In addition, during awake immobility in the rest environment, the N unit population showed a dominant coupling to the N wave network pattern, suggesting similar or equivalent circuit mechanisms underlying spatial firing during immobility in quiescent conditions as spatial firing during immobility in the task (Extended Data Fig. 10m).

Discussion

These findings identify a distinct hippocampal network at the anatomical (Fig. 1), behavioural (Fig. 2), representational (Fig. 3), and neural

© 2016 Macmillan Publishers Limited. All rights reserved

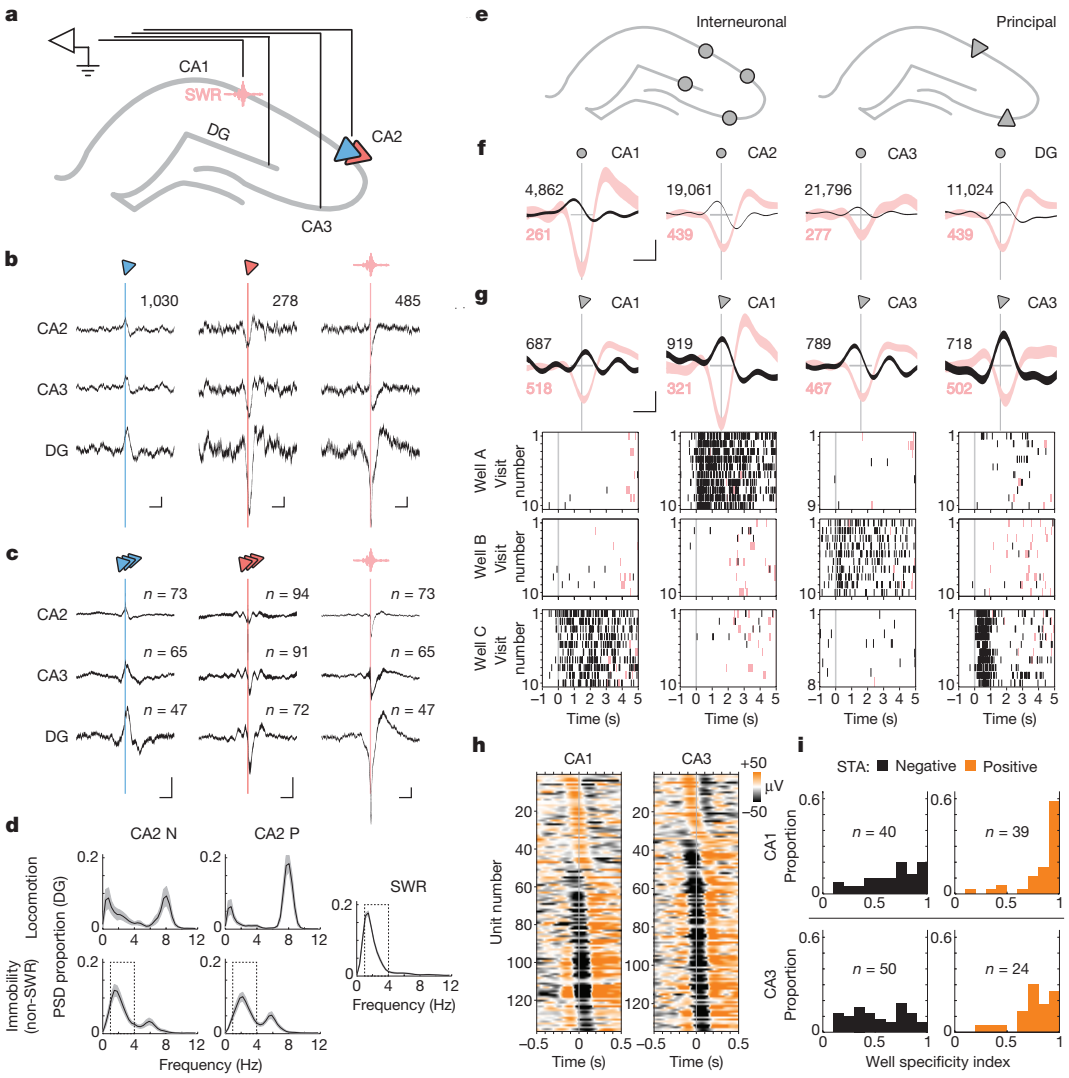


Figure 4 | A novel hippocampal network pattern marks spatial coding during immobility. a, Schematic of recording configuration. SWRs (pink symbol) were detected with CA1 site electrodes, while wide-band LFP was taken from CA2, CA3, and DG site electrodes. Blue and red symbols refer to CA2 N and CA2 P units, respectively, analysed in **b**–**d**. **b**, Example CA2 N (blue symbol, first column) and CA2 P (red symbol, second column) unit spike-triggered average (STA) and SWR-triggered average (RTA; pink symbol, third column) of hippocampal CA2, CA3, and DG LFP from non-SWR immobility periods. Vertical lines indicate the time of spiking (STA) or time of SWR (RTA). The two units were recorded simultaneously and on the same tetrode. SWRs averaged in the RTA were detected in the same recording epochs as the units. The total number of events averaged is reported at upper right. Trace width indicates ± s.e.m. over single LFP traces. Trace length: 2 s. Scale bars: *x*, 250 ms; *y*, 100 μV. **c**, Mean STAs for CA2 N and CA2 P unit populations for non-SWR immobility periods. The mean RTA was calculated from single RTAs matching the recording epochs of N unit STAs, and thus have the same sample size. Trace width indicates ± s.e.m. over unit STAs/RTAs. Trace length: 2 s. Scale bars: *x*, 250 ms; *y*, 100 μV. **d**, Power spectral density (PSD) of STAs and RTAs of DG LFP. The mean PSD is plotted as a black line, with ± s.e.m. over single averages plotted in grey (locomotor periods: CA2 N, $n = 39$ units; CA2 P, $n = 85$; non-SWR immobility periods: CA2 N, $n = 47$; CA2 P, $n = 72$; RTAs matched to CA2 N units: $n = 47$). **e**, Schematic of additional hippocampal neurons analysed with STAs. Interneuronal units (left, grey circles) recorded in the principal cell layers of CA1, CA2, CA3 and DG analysed in **f** and Extended Data Fig. 7d–g. Principal units (right, grey triangles) recorded in CA1 and CA3 analysed in **g**–**i** and Extended Data Figs 8 and 9. STAs in **f**–**i** were taken for 1–4 Hz LFP, analysing spikes from non-SWR immobility periods. **f**, N wave firing in four example interneuronal units. Plotted are unit STAs and RTAs. Trace width indicates ± s.e.m. (STA, black) or ± 2 s.e.m. (RTA, pink) over single LFP traces. Vertical line: time of spiking (STAs) or SWRs (RTAs). The hippocampal subregion in which the unit was recorded is reported at upper right. The number of spikes or SWRs averaged is indicated at upper and lower left, respectively. Trace length: 1 s. Horizontal line (200 ms in length): 0 μV. DG LFP was used in each example except for the CA3 unit, which used CA3 LFP. Scale bars: *x*, 200 ms; *y*, 50 μV for STA, 100 μV for RTA. **g**, N wave firing and well specificity in four example CA1/CA3 principal units. Top: unit STAs and RTAs, following the plotting conventions in **f**. DG LFP was used in each example. Bottom: well firing rasters correspondent with each unit. Grey line: time of well entry ($t = 0$). SWR periods plotted as pink zones. **h**, CA1 and CA3 unit STAs. Colour indicates voltage. For each unit, LFP (1–4 Hz) from DG, CA3, or CA2 (in decreasing order of preference) was used. Unit STAs were grouped by polarity at the time of spiking ($t = 0$) and sorted by the time of the local extremum (peak for positive; trough for negative) nearest the time of spiking. Units with positive voltage peaks at the time of spiking were classified as N wave-coupled. **i**, Well specificity distributions for CA1 and CA3 principal unit populations classified by STA. For both CA1 and CA3 populations, units with positive STAs (N wave-coupled) showed higher well specificity than units with negative STAs (mean ± s.e.m.; CA1 positive: 0.85 ± 0.03; CA1 negative: 0.65 ± 0.04, CA1 positive versus CA1 negative, $P < 10^{-5}$, rank-sum; CA3 positive: 0.77 ± 0.04; CA3 negative: 0.53 ± 0.04, CA3 positive versus CA3 negative, $P < 0.001$, rank-sum).

© 2016 Macmillan Publishers Limited. All rights reserved

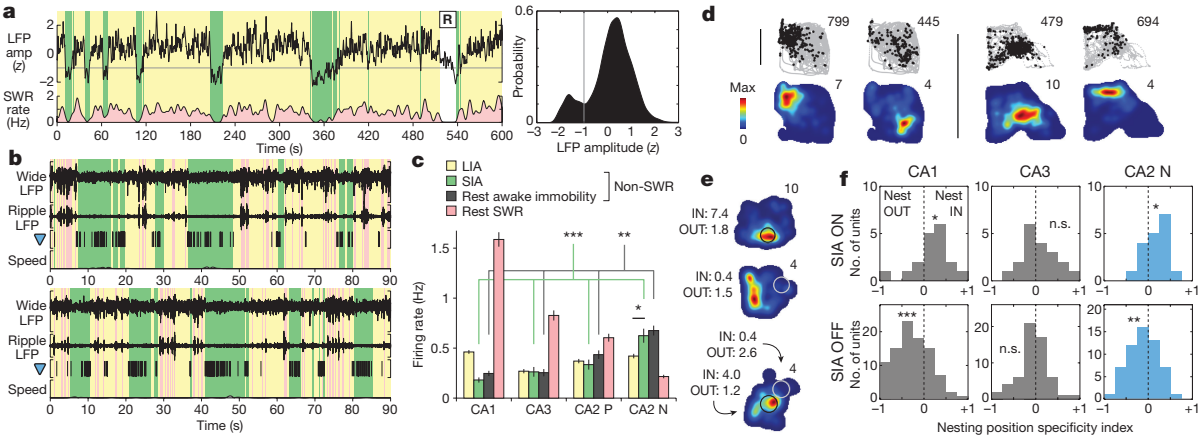


Figure 5 | Hippocampal spatial coding in desynchronized sleep. **a**, Detection of sleep states using hippocampal LFP. Left, 10-min trace of aggregate hippocampal LFP amplitude during sleep, with times classified as LIA (yellow), SIA (green), or REM (R) periods. SWR rate was estimated by counting SWRs in 1-s bins and smoothing with a Gaussian ($\sigma = 2$ s). Right, kernel density estimate (Gaussian kernel, $\sigma = 0.1$) of aggregate hippocampal LFP amplitude during non-REM sleep for the recording epoch from which the plotted trace was taken. Grey line: amplitude threshold used to distinguish SIA (below threshold) and LIA (above threshold) periods. **b**, Sleep firing in two example CA2 N units. Top traces: wide-band LFP (Wide, 0.5–400 Hz, scale bar: 2 mV) and ripple-band LFP (Ripple, 150–250 Hz, scale bar: 300 μV) traces from a simultaneous recording in CA1. SWR, LIA, and SIA periods are plotted as pink, yellow, and green zones, respectively. Grey-filled trace (*y* axis: 0 to 10 cm s^{-1}): head speed. Subsequent analysis in **d**–**f** indicated that SIA firing was dependent on whether the location at which the animal slept was near the spatial firing field of the CA2 N unit. **c**, Mean firing rates during rest epochs (mean ± s.e.m.; number of units: CA1: 400, CA3: 220, CA2 P: 126 units, CA2 N: 76 units). CA2 N units fired more during SIA than LIA ($P = 0.011$, signed-rank) and at higher rates than other unit populations during SIA periods (green) and during awake immobility periods (grey) (Kruskal–Wallis ANOVA, Tukey's post hoc tests; $P < 0.001$ for SIA; $P = 0.0051$ for awake immobility). As in Fig. 2c, these comparisons indicate population-level engagement in sleep states, encompassing both higher and lower rate firing as a result of spatially specific firing in single units. $^*P < 0.05$; $^{**}P < 0.01$; $^{***}P < 0.001$. **d**, Example spatial firing maps of two pairs of simultaneously recorded CA2 N units in the rest environment. Data from waking periods plotted. Upper plots: positions visited (grey) and positions where the unit fired (black points). Total number of spikes is reported at upper right. Lower plots: occupancy-normalized firing maps. Peak spatial firing rate is reported at upper right. Scale bar: 20 cm. **e**, Three example CA2 N units coding for nesting position. Shown are occupancy-normalized firing maps from awake periods in a rest recording epoch. Indicated on each map is the nesting position (circle, 5 cm radius) of the subject for a sleep period detected in the same recording epoch. For a given sleep period, the unit was classified either as SIA ON (>2 Hz firing rate during SIA; black circle) or SIA OFF (<2 Hz; white circle). Reported at left are the mean awake firing rates within (Nest IN) and outside (Nest OUT) the encircled nesting region. In the third example, two distinct nesting positions corresponding to two distinct sleep periods were observed. **f**, Nesting position specificity index distribution in CA1, CA3, and CA2 N unit populations. The CA1 and CA2 N populations met dual criteria (see Methods) for nesting position coding, while the CA3 unit population did not. Mean ± s.e.m.: CA1, SIA ON ($n = 18$ units): 0.18 ± 0.09, $P = 0.043$; CA1, SIA OFF ($n = 92$): -0.26 ± 0.04, $P < 10^{-6}$; CA3, SIA ON ($n = 19$): 0.09 ± 0.09, $P = 0.47$; CA3, SIA OFF ($n = 58$): -0.04 ± 0.04, $P = 0.50$; CA2 N, SIA ON ($n = 18$): 0.18 ± 0.06, $P = 0.020$; CA2 N, SIA OFF ($n = 57$): -0.12 ± 0.04, $P = 0.0087$. All statistical tests were signed-rank. $^*P < 0.05$; $^{**}P < 0.01$; $^{***}P < 0.001$; n.s., not significant at $P < 0.05$.

circuit (Figs 1 and 4) levels, and also indicate its activation in sleep (Fig. 5). In the awake animal, neural firing in this network is marked by a distinct hippocampal network pattern (N wave), occurs during immobility in subsets of neurons in CA1, CA2, CA3, and DG, and is location-specific, constituting an explicit neural code for current position. Thus the classic locomotor hippocampal place code switches, during immobility, to an alternative hippocampal neural code that nonetheless maintains spatial specificity.

Past observations of a lack of place cell firing in restrained animals have led to the suggestion that place firing is driven by input correspondent with an animal's preparedness to make limb movements that would displace the animal from its current position, a condition termed 'motor set'[38,39]. Moreover, in rodents, hippocampal theta has been proposed to be a marker of motor set[1,34,40], and thus by inference a marker of hippocampal place firing. Here we observe spatial firing dependent on neither theta nor motor set, indicating that distinct mechanisms can generate spatial firing and in fact do so complementarily.

A neural code for location during awake immobility enables the brain to provide a spatial context to events occurring during immobility such as consumption of food, sensory stimuli, and deliberation, allowing for the formation of location-specific memories when the animal is still. Moreover, we suggest that the various hippocampus-dependent behaviours characterized by immobility[1,5–10] engage this network, and that activity in this network may correspond to activity seen in human[41], monkey[42], and bat[43] hippocampus, where the theta network pattern occurs less frequently. Importantly, analysis of firing during immobility has not been prominent in traditional approaches to hippocampal spatial coding, in which behavioural paradigms eliciting continuous locomotion or post hoc exclusion of immobility periods is the norm.

Remarkably, a distinct population of hippocampal neurons located at CA2 (N units) signalled location during not only awake immobility but also sleep. An internal representation of current location active during sleep could adaptively influence representations reactivated in sleep in support of memory consolidation[44–46], and, concurrently, could serve to maintain a sleeping animal's bearings despite diminished receptivity to sensory stimuli.

Finally, the localization of N units at CA2 suggests that N units correspond to CA2 neurons, while CA2 P units correspond to intermingling CA1 and CA3 neurons at the CA2 anatomical locus. In parallel with the unique firing pattern of N units, CA2 neurons exhibit a variety of properties unique among hippocampal neurons, including a unique synaptic configuration[35–37,47,48]. Moreover, a recent study reports suppressed firing in three identified CA2 neurons during SWRs[49], indicating that N units and CA2 neurons are overlapping populations or in fact identical. Recent work also links CA2 neurons to the generation of time-dependent spatial representations[28], spatial pattern completion[29,30], and social memory[37]. These cognitive functions and possibly others may rely on the alternative forms of hippocampal neural activity identified here.

Online Content Methods, along with any additional Extended Data display items and Source Data, are available in the online version of the paper; references unique to these sections appear only in the online paper.

© 2016 Macmillan Publishers Limited. All rights reserved

Received 9 June 2015; accepted 13 January 2016.
Published online 2 March 2016.

1. O'Keefe, J. & Nadel, L. *The Hippocampus as a Cognitive Map* (Oxford Univ. Press, 1978).
2. Wilson, M. A. & McNaughton, B. L. Dynamics of the hippocampal ensemble code for space. *Science* **261,** 1055–1058 (1993).
3. Buzsáki, G. & Moser, E. I. Memory, navigation and theta rhythm in the hippocampal-entorhinal system. *Nature Neurosci.* **16,** 130–138 (2013).
4. Eichenbaum, H. & Cohen, N. J. Can we reconcile the declarative memory and spatial navigation views on hippocampal function? *Neuron* **83,** 764–770 (2014).
5. Eilam, D. & Golani, I. Home base behavior of rats (*Rattus norvegicus*) exploring a novel environment. *Behav. Brain Res.* **34,** 199–211 (1989).
6. Wallace, D. G., Hamilton, D. A. & Whishaw, I. Q. Movement characteristics support a role for dead reckoning in organizing exploratory behavior. *Anim. Cogn.* **9,** 219–228 (2006).
7. Bannerman, D. M. *et al.* Regional dissociations within the hippocampus—memory and anxiety. *Neurosci. Biobehav. Rev.* **28,** 273–283 (2004).
8. Pentkowski, N. S., Blanchard, D. C., Lever, C., Litvin, Y. & Blanchard, R. J. Effects of lesions to the dorsal and ventral hippocampus on defensive behaviors in rats. *Eur. J. Neurosci.* **23,** 2185–2196 (2006).
9. Maren, S., Phan, K. L. & Liberzon, I. The contextual brain: implications for fear conditioning, extinction and psychopathology. *Nature Rev. Neurosci.* **14,** 417–428 (2013).
10. Christian, K. M. & Thompson, R. F. Neural substrates of eyeblink conditioning: acquisition and retention. *Learn. Mem.* **10,** 427–455 (2003).
11. Takahashi, M., Lauwereyns, J., Sakurai, Y. & Tsukada, M. A code for spatial alternation during fixation in rat hippocampal CA1 neurons. *J. Neurophysiol.* **102,** 556–567 (2009).
12. MacDonald, C. J., Carrow, S., Place, R. & Eichenbaum, H. Distinct hippocampal time cell sequences represent odor memories in immobilized rats. *J. Neurosci.* **33,** 14607–14616 (2013).
13. Hattori, S., Chen, L., Weiss, C. & Disterhoft, J. F. Robust hippocampal responsivity during retrieval of consolidated associative memory. *Hippocampus* **25,** 655–669 (2015).
14. Carr, M. F., Jadhav, S. P. & Frank, L. M. Hippocampal replay in the awake state: a potential substrate for memory consolidation and retrieval. *Nature Neurosci.* **14,** 147–153 (2011).
15. Pfeiffer, B. E. & Foster, D. J. Hippocampal place-cell sequences depict future paths to remembered goals. *Nature* **497,** 74–79 (2013).
16. Buzsáki, G., Horvath, Z., Urioste, R., Hetke, J. & Wise, K. High-frequency network oscillation in the hippocampus. *Science* **256,** 1025–1027 (1992).
17. Buzsáki, G. Hippocampal sharp wave-ripple: a cognitive biomarker for episodic memory and planning. *Hippocampus* **10,** 1073–1188 (2015).
18. Buzsáki, G., Leung, L. W. & Vanderwolf, C. H. Cellular bases of hippocampal EEG in the behaving rat. *Brain Res.* **6,** 139–171 (1983).
19. Csicsvari, J., Hirase, H., Mamiya, A. & Buzsaki, G. Ensemble patterns of hippocampal CA3–CA1 neurons during sharp wave-associated population events. *Neuron* **28,** 585–594 (2000).
20. Penttonen, M., Kamondi, A., Sik, A., Acsady, L. & Buzsaki, G. Feed-forward and feed-back activation of the dentate gyrus *in vivo* during dentate spikes and sharp wave bursts. *Hippocampus* **7,** 437–450 (1997).
21. Karlsson, M. P. & Frank, L. M. Awake replay of remote experiences in the hippocampus. *Nature Neurosci.* **12,** 913–918 (2009).
22. Davidson, T. J., Kloosterman, F. & Wilson, M. A. Hippocampal replay of extended experience. *Neuron* **63,** 497–507 (2009).
23. Gupta, A. S., van der Meer, M. A., Touretzky, D. S. & Redish, A. D. Hippocampal replay is not a simple function of experience. *Neuron* **65,** 695–705 (2010).
24. Kim, S. M. & Frank, L. M. Hippocampal lesions impair rapid learning of a continuous spatial alternation task. *PLoS ONE* **4,** e5494 (2009).
25. McNaughton, B. L., Barnes, C. A. & O'Keefe, J. The contributions of position, direction, and velocity to single unit activity in the hippocampus of freely-moving rats. *Exp. Brain Res.* **52,** 41–49 (1983).
26. Huxter, J., Burgess, N. & O'Keefe, J. Independent rate and temporal coding in hippocampal pyramidal cells. *Nature* **425,** 828–832 (2003).
27. Zheng, C., Bieri, K. W., Trettel, S. G. & Colgin, L. L. The relationship between gamma frequency and running speed differs for slow and fast gamma rhythms in freely behaving rats. *Hippocampus* **25,** 924–938 (2015).
28. Mankin, E. A., Diehl, G. W., Sparks, F. T., Leutgeb, S. & Leutgeb, J. K. Hippocampal CA2 activity patterns change over time to a larger extent than between spatial contexts. *Neuron* **85,** 190–201 (2015).
29. Lu, L., Igarashi, K. M., Witter, M. P., Moser, E. I. & Moser, M. B. Topography of place maps along the CA3-to-CA2 axis of the hippocampus. *Neuron* **87,** 1078–1092 (2015).
30. Lee, H., Wang, C., Deshmukh, S. S. & Knierim, J. J. Neural population evidence of functional heterogeneity along the CA3 transverse axis: pattern completion versus pattern separation. *Neuron* **87,** 1093–1105 (2015).
31. Mizuseki, K., Sirota, A., Pastalkova, E. & Buzsaki, G. Theta oscillations provide temporal windows for local circuit computation in the entorhinal-hippocampal loop. *Neuron* **64,** 267–280 (2009).
32. Buzsáki, G. Hippocampal sharp waves: their origin and significance. *Brain Res.* **398,** 242–252 (1986).
33. Jarosiewicz, B., McNaughton, B. L. & Skaggs, W. E. Hippocampal population activity during the small-amplitude irregular activity state in the rat. *J. Neurosci.* **22,** 1373–1384 (2002).
34. Vanderwolf, C. H. Hippocampal electrical activity and voluntary movement in the rat. *Electroencephalogr. Clin. Neurophysiol.* **26,** 407–418 (1969).
35. Chevaleyre, V. & Siegelbaum, S. A. Strong CA2 pyramidal neuron synapses define a powerful disynaptic cortico-hippocampal loop. *Neuron* **66,** 560–572 (2010).
36. Kohara, K. *et al.* Cell type-specific genetic and optogenetic tools reveal hippocampal CA2 circuits. *Nature Neurosci.* **17,** 269–279 (2014).
37. Hitti, F. L. & Siegelbaum, S. A. The hippocampal CA2 region is essential for social memory. *Nature* **508,** 88–92 (2014).
38. Foster, T. C., Castro, C. A. & McNaughton, B. L. Spatial selectivity of rat hippocampal neurons: dependence on preparedness for movement. *Science* **244,** 1580–1582 (1989).
39. McNaughton, B. L., Battaglia, F. P., Jensen, O., Moser, E. I. & Moser, M. B. Path integration and the neural basis of the 'cognitive map'. *Nature Rev. Neurosci.* **7,** 663–678 (2006).
40. Buzsáki, G. Theta rhythm of navigation: link between path integration and landmark navigation, episodic and semantic memory. *Hippocampus* **15,** 827–840 (2005).
41. Watrous, A. J. *et al.* A comparative study of human and rat hippocampal low-frequency oscillations during spatial navigation. *Hippocampus* **23,** 656–661 (2013).
42. Jutras, M. J., Fries, P. & Buffalo, E. A. Oscillatory activity in the monkey hippocampus during visual exploration and memory formation. *Proc. Natl Acad. Sci. USA* **110,** 13144–13149 (2013).
43. Ulanovsky, N. & Moss, C. F. Hippocampal cellular and network activity in freely moving echolocating bats. *Nature Neurosci.* **10,** 224–233 (2007).
44. Lee, A. K. & Wilson, M. A. Memory of sequential experience in the hippocampus during slow wave sleep. *Neuron* **36,** 1183–1194 (2002).
45. Girardeau, G., Benchenane, K., Wiener, S. I., Buzsaki, G. & Zugaro, M. B. Selective suppression of hippocampal ripples impairs spatial memory. *Nature Neurosci.* **12,** 1222–1223 (2009).
46. Ego-Stengel, V. & Wilson, M. A. Disruption of ripple-associated hippocampal activity during rest impairs spatial learning in the rat. *Hippocampus* **20,** 1–10 (2010).
47. Dudek, S. M., Alexander, G. M. & Farris, S. Rediscovering area CA2: unique properties and functions. *Nature Rev. Neurosci.* **17,** 89–102 (2016).
48. Rowland, D. C. *et al.* Transgenically targeted rabies virus demonstrates a major monosynaptic projection from hippocampal area CA2 to medial entorhinal layer II neurons. *J. Neurosci.* **33,** 14889–14898 (2013).
49. Valero, M. *et al.* Determinants of different deep and superficial CA1 pyramidal cell dynamics during sharp-wave ripples. *Nature Neurosci.* **18,** 1281–1290 (2015).
50. Lorente de Nó, R. Studies on the structure of the cerebral cortex. *II. Continuation of the study of the ammonic system. Journal für Psychologie und Neurologie.* **46,** 113–177 (1934).

Acknowledgements We thank G. Rothschild, D. Liu, J. Yu, S. Jadhav, E. Anderson, P. Sabes, C. Schreiner, M. Stryker, R. Knight, J. O'Doherty, E. Phillips, K. Kay, and B. Mensh for discussion and suggestions, and I. Grossrubatscher, C. Lykken, and S. Harris for technical assistance. This work was supported by the Howard Hughes Medical Institute, an NIH grant (R01 MH090188) and a McKnight Foundation Cognitive and Memory Disorders Award (L.M.F.). K.K. is supported by a Ruth L. Kirchstein National Research Service Award Fellowship (NIH/NIMH) and the UCSF Medical Scientist Training Program.

Author Contributions K.K. and L.M.F. conceived the study. K.K., M.S., J.E.C., M.P.K., and M.C.L., conducted the experiments. K.K. analysed the data. K.K. and L.M.F. wrote the paper.

Author Information Reprints and permissions information is available at www.nature.com/reprints. The authors declare no competing financial interests. Readers are welcome to comment on the online version of the paper. Correspondence and requests for materials should be addressed to K.K. (kenneth.kay@ucsf.edu) or L.M.F. (loren@phy.ucsf.edu).

© 2016 Macmillan Publishers Limited. All rights reserved

METHODS

Data reporting. No statistical methods were used to predetermine sample size. The investigators were not blinded to allocation during experiments and outcome assessment.

Subjects, neural recordings, and behavioural task. Eight male Long-Evans rats that were 4 to 9 months old (500–600 g) were food deprived to 85% of their baseline weight and pre-trained to run on a 1-m linear track for liquid reward (sweetened evaporated milk). After subjects alternated reliably, they were implanted with microdrives containing 14 (two subjects), 21 (three subjects), or 30 (three subjects) independently movable four-wire electrodes (tetrodes[2,51]) targeting dorsal hippocampus (all subjects) and medial entorhinal cortex (one subject), in accordance with University of California San Francisco Institutional Animal Care and Use Committee and US National Institutes of Health guidelines. The minimum number of subjects was established beforehand as four or more, as this is considered to be the minimum necessary to yield data with sufficient statistical power to evaluate the type of effects investigated in this study.

In two subjects, right and left dorsal hippocampus were targeted at AP: −3.7 mm, ML: ± 3.7 mm. In one subject, dorsal hippocampus was targeted at AP: −3.6 mm, ML: +2.2 mm, in addition to medial entorhinal cortex at AP: −9.1, ML: +5.6, at a 10 degree angle in the sagittal plane. Data from these several subjects have been reported in earlier studies[21,63]. In five subjects, right dorsal hippocampus was targeted at AP: −3.3 to −4.0 mm, ML: +3.5 to +3.9 mm, moreover, in two of these subjects, the septal pole of right hippocampus was targeted with an additional six tetrodes targeted to AP: −2.3 mm, ML: +1.1 mm. Targeting locations were used to position stainless steel cannulae containing 6, 14, 15, or 21 independently driveable tetrodes. The cannulae were circular except in four cases targeting dorsal hippocampus in which they were elongated into ovals (major axis ∼2.5 mm, minor axis ∼1.5 mm; two subjects with major axis 45° relative to midline, along the transverse axis of dorsal hippocampus; two subjects with major axis 135° relative to midline, along the longitudinal axis of dorsal hippocampus). Data exclusively from tetrodes targeting right dorsal hippocampus were analysed in this study.

In five subjects, viral vectors with optogenetic transgenes were targeted to either right dorsal CA2 (three subjects, AAV2/5-CaMKII-hChR2(H134R)-EYFP, UNC Vector Core, 135 nl at AP: −3.6 mm, ML: +4.2 mm, DV: −4.5 mm), dorsal DG (one subject, AAV2/5-I12B-ChR2-GFP (see ref. 52 for details about the I12B promoter)), 225 nl at AP: −3.75 mm, ML: +2.2 mm, DV: 3.9 mm and AP: −3.75 mm, ML: +1.8 mm, DV: −4.5 mm), or right supramammilary nucleus (one subject, AAV2/5-hSyn-ChETA-EYFP, Penn Vector Core, 135 nl at AP: −4.3 mm, ML: +1.8 mm, and −8.9 mm along a trajectory angled at 6° in the coronal plane). Viruses were delivered during the implant surgery using a glass micropipette (tip manually cut to ∼25 μm diameter) attached to an injector (Nanoject, Drummond Scientific). In addition, a driveable optical fibre (62.5/125 μm core/cladding) was integrated in the tetrode microdrive assembly to enable light delivery to hippocampus. This fibre was advanced to its final depth (2.5–3 mm) within 7 days of implantation. Data reported in this study were collected before light stimulation. No overt differences in neural activity were observed in subjects that received virus. In particular, CA2 recording sites reporting heterogeneous unit populations (Extended Data Fig. 3c) were found in subjects either receiving or free of viral vectors.

Over the course of two weeks following implantation, the tetrodes were advanced to the principal cell layers of CA1 (all subjects), CA2 (5 subjects), CA3 (all subjects), and DG (3 subjects). For DG, tetrodes were advanced to the cell layer using a previously described protocol in which the tetrodes were slowly advanced within DG (∼10 μm increments) and unit activity monitored over long periods of rest[53]. DG cell layer was identified by the presence of highly sparsely firing putative principal units. In several subjects, tetrodes were also left in cortex overlying dorsal hippocampus. Neural signals were recorded relative to a reference (REF) tetrode positioned in corpus callosum above right dorsal hippocampus. The REF tetrode reported voltage relative to a ground screw installed in skull overlying cerebellum, and local field potential (LFP) from this tetrode was also recorded. All tetrode final locations were histologically verified (see below).

After 5–7 days of recovery after surgery, subjects were once again food deprived to 85% of their baseline weight, and again pre-trained to run on a linear track for liquid reward. At ∼14 days after surgery, six subjects were then introduced to one task W-maze (Extended Data Fig. 1a) and recorded for 3 to 6 days before being introduced to a second task W-maze, located in a separate part of the recording room and rotated 90° relative to the first. On recording days in which the second task W-maze was used, recordings were also conducted in the first task W-maze. In two subjects, recordings were conducted in both task W-mazes on every recording day. The W-mazes were 76 × 76 cm with 7-cm-wide track sections. The two task W-mazes were separated by an opaque barrier.

In each W-maze, subjects were rewarded for performing a hippocampus-dependent continuous alternation task[21,24,65,70] (Extended Data Fig. 1a). Liquid reward (sweetened evaporated milk) was dispensed via plastic tubing connected to a hole at the bottom of each of the three reward wells (wells A, B, and C), miniature bowls 3 cm in diameter. In three subjects, reward was dispensed via syringes operated manually by an experimenter who was located in a separate part of the recording room. In five subjects, entry of the subject's head into reward wells was sensed by an infrared beam break circuit attached to the well, and reward was automatically delivered by syringe pumps (OEM syringe pumps, Braintree Scientific) either immediately or after an imposed delay lasting from 0.5 to 2 s. In these subjects, digital time stamps corresponding to well entry and reward delivery were recorded and used for illustration in Fig. 3c, but were otherwise not used in determining entry times or occupancy of the subjects at the wells for consistency among all subjects. Task epochs lasting 15 min were preceded and followed by rest epochs lasting ∼20 min in a high-walled black box (floor edges 25–35 cm and height 50 cm), during which rats often groomed, quietly waited, and slept. Two subjects also ran in an open field environment for scattered food (grated cheese) after W-maze recordings, with additional interleaved rest epochs. Tetrode positions were adjusted after each day's recordings.

Data were collected using the NSpike data acquisition system (L.M.F. and J. MacArthur, Harvard Instrumentation Design Laboratory). During recording, an infrared diode array with a large and a small cluster of diodes was affixed to headstage preamplifiers to enable tracking of head position and head direction. Following recording, position and direction were reconstructed using a semi-automated analysis of digital video (30 Hz) of the experiment. Spike data were recorded relative to the REF tetrode, sampled at 30 kHz, digitally filtered between 600 Hz and 6 kHz (2-pole Bessel for high- and low-pass), and threshold crossing events were saved to disk. Local field potentials (LFPs) were sampled at 1.5 kHz and digitally filtered between 0.5 Hz and 400 Hz. LFPs analysed were relative to the REF tetrode except where otherwise indicated.

Individual units (putative single neurons) were identified by clustering spikes using peak amplitude, principal components, and spike width as variables (MatClust, M.P.K.). Only well-isolated neurons with stable spike waveform amplitudes were clustered. A single set of cluster bounds defined in amplitude and width space could often isolate units across an entire recording session. In cases where there was a shift in amplitudes across time, units were clustered only when that shift was coherent across multiple clusters and when plots of amplitude versus time showed a smooth shift. No units were clustered in which part of the cluster was cut off at spike threshold.

Histology and recording site assignment. After recordings, subjects were anesthetized with isoflurane, electrolytically lesioned at each tetrode (30 μA of positive current for 3 s applied to two channels of each tetrode), and allowed to recover overnight. In one subject, no electrolytic lesions were made, and tetrode tracks rather than lesions were used to identify recording sites. Subjects were euthanized with pentobarbital and were perfused intracardially with PBS followed by 4% paraformaldehyde in PBS. The brain was post-fixed *in situ* overnight, after which the tetrodes were retracted and the brain removed, cryo-protected (30% sucrose in PBS), and embedded in OCT compound. Coronal (7 subjects) and sagittal (1 subject) sections (50 μm) were taken with a cryostat. Sections were either Nissl-stained with cresyl violet or stained with the fluorescent Nissl reagent NeuroTrace Blue (1:200) (Life Technologies, N-21479). In four subjects, the sections were blocked (5% donkey serum in 0.3% Triton-X in TBS, used for all incubations) for 1 h, incubated with RGS14 (refs 36, 47, 71) antibody (1:400) (Antibodies Inc., 75-140) overnight, washed, and subsequently incubated with fluorescent secondary antibody (1:400) (Alexa 568, Life Technologies). CA2 recording sites were designated as those in which the electrolytic lesion or end of tetrode track overlapped with the dispersed cytoarchitectural zone characteristic of CA2 (refs 28–30, 47, 50, 54–57). This strategy was deliberately inclusive to maximize detection of putative CA2 neurons with novel physiological responses (N units, Fig. 1 and Extended Data Fig. 3). It is important to note that CA2 sites defined in this way include recording locations that have been designated in previous studies as 'CA3a'.

Data analysis. All analyses were carried out using custom software written in Matlab (Mathworks).

SWR detection. Detection of SWRs was prerequisite for all data analysed in this study, and was performed only when at least three CA1 cell layer recordings were available. Offline, a multisite average approach was used to detect SWRs[58]. Specifically, LFPs from all available CA1 cell layer tetrodes were filtered between 150–250 Hz, then squared and summed across tetrodes. This sum was smoothed with a Gaussian kernel ($\sigma = 4$ ms) and the square root of the smoothed sum was analysed. SWRs were detected when the signal exceeded 2 s.d. of the recording epoch mean for at least 15 ms. SWR periods were then defined as the periods,

© 2016 Macmillan Publishers Limited. All rights reserved

containing the times of threshold crossing, in which the power trace exceeded the mean. SWR onset was defined as the start of a SWR period. Detection of SWRs was performed only when subjects' head speed was $<4\,cm\,s^{-1}$. For SWR-triggered spike raster plots and PSTH plots, a 0.5 s exclusion period was imposed to isolate SWRs occurring only after non-SWR periods; otherwise, analyses of SWRs included all detected SWRs.

Unit inclusion. Two unit sets were analysed in this study. In the first (task unit set), units included fired at least 100 spikes outside of SWRs in at least one task epoch. In the second set (rest unit set), units included fired at least 100 spikes outside of SWRs in at least one rest epoch, moreover specifically in awake periods (see below). The rest unit set was established to evaluate spatial representations and network patterns in the rest environment. For both unit sets, all included units were required to have available data for least 300 (typically >1,000) concurrently detected SWRs in either task or rest epochs. Since relatively less is understood about hippocampal neurons in CA2, units recorded at CA2 in the rest unit set were included in the study only if they met the task unit set criterion to ensure that neurons engaged during active behaviour were evaluated. All unit population findings in this study refer to the task unit set, with the exception of those presented in Fig. 5f and Extended Data Fig. 10, which refer to the rest unit set.

Principal versus interneuronal unit classification. For each unit set, scatter plots of firing rate, spike width, and autocorrelation function mean (calculated from 0 to 40 ms; low values indicating burst firing) showed two distinct clusters[18,31,59–62] (example plot of task unit set in Fig. 1c). Putative principal units corresponded with the low firing rate (<4 Hz), large spike width, low autocorrelation mean cluster, while putative interneuronal units corresponded to the cluster characterized by high firing rate, small spike width, and high autocorrelation mean. Twenty-one units with ambiguous features were left unclassified. All units in the study were isolated (clustered) and classified before STA analysis.

N versus P unit classification. Periods when head speed was $<4\,cm\,s^{-1}$ were segregated into SWR versus non-SWR periods, and the change in firing rate during SWRs calculated. The period types were then permuted ($n=1{,}000$) to obtain a distribution of firing rate differences given the null hypothesis of no association of firing rate with period type. P units were those units showing a difference in firing rate that was >95% of values from the null distribution, either for SWRs of any single task epoch or for rest epoch SWRs. N units were those that showed a failure of significance for SWRs in every task epoch and also for rest epoch SWRs. This approach minimized false positives in the detection of N units. Negatively modulated (inhibited) units were formally identified as a subset of N units (examples in Fig. 1c, d and additional observations in Extended Data Fig. 3b) showing a firing rate difference during SWRs that was <95% of the values from the null hypothesis distribution for rest epoch SWRs and also for SWRs of at least one task epoch.

A small number of CA1 principal units (11 out of 504) and CA3 principal units (7 out of 289) were classified as N units (N versus P proportions for the task unit set shown in Fig. 1e); these units were excluded from all analyses. After exclusion of N units for CA1 and CA3, total putative principal unit counts in the task unit set were CA1: 478, CA3: 271, CA2 P: 142, CA2 N: 84; in the rest unit set, CA1: 163, CA3: 76, CA2 P: 76, CA2 N: 68. Throughout this study, 'N units' and 'P units' solely refer to the distinct unit populations recorded at CA2 sites, and are equivalent to 'CA2 N' and 'CA2 P'.

Behavioural state. Periods of locomotion were defined as times when head speed was $>4\,cm\,s^{-1}$. Periods of non-SWR immobility were times when head speed was $<4\,cm\,s^{-1}$ separated from locomotor periods by 2 s buffer intervals (preceding and following) and excluding SWR periods. Thus brief interruptions in locomotion did not qualify as formally detected periods of immobility.

Firing rate estimation. For each unit, instantaneous firing rate (IFR) was estimated by convolving the unit's spike train (1-ms bins) with a Gaussian kernel ($\sigma=250$ ms). Mean firing rates in the task (Fig. 2c and Extended Data Fig. 8b) were calculated from the task epoch in which the unit had the highest mean firing rate combined with additional task epochs of the same environment (specific W-maze) when available. Mean firing rates in the rest environment (Fig. 5c) were calculated from all available rest epochs, and were only calculated for units for which LIA and SIA sleep data were available. Firing rates during SWRs were calculated for SWR periods in either task epochs (Fig. 2c and Extended Data Fig. 8b) or rest epochs (Fig. 5c).

Firing versus speed correlation. For each unit, the Pearson correlation coefficient (r) was calculated between IFR and the logarithm of head speed[27,63,64] for non-SWR periods. The correlation was calculated from the task epoch in which the unit had the highest mean firing rate combined with additional task epochs of the same W-maze when available. Only units with significant correlations ($P<0.05$) were analysed (CA1: 475/477 units, CA2 P: 141/142 units, CA2 N: 83/84 units, CA3: 270/271 units). It is worth noting that the findings relating CA2 N unit firing to speed in the task condition (Fig. 2) are not a direct consequence of the N unit classification criteria, which refer strictly to a lack of increased firing during SWRs.

Spatial firing. To quantify spatial coverage, 2D position data (corresponding to subjects' head location) for all subjects was first converted to linear position. Linear position was measured as the distance from the centre reward well along the linear arms of the W-shaped task maze. In addition, all linear positions were classified as belonging to one of four possible trajectories of the behavioural task, namely, outbound and inbound trajectories between the centre well and each of the two outer wells (diagrammed in Extended Data Fig. 1a). The end of each continuous trajectory assignment period corresponded to the separation of the subject's linear position from that of the target well of the given trajectory (>2 cm from well).

No trajectory assignment was performed for periods of data corresponding to three cases: (1) excursions in which in the subject departed and returned to the same well, (2) excursions in which the subject occupied a maze segment that was not part of the three linear segments defining the animal's current trajectory, and (3) times during which the subject's linearized head direction (either forward or backward along the current maze segment) did not match the defined direction of the animal's current trajectory. These unassigned periods represented a minority proportion of the data (33% across all task sessions) and were not included either in spatial plots referencing trajectory (occupancy-normalized firing maps in Extended Data Fig. 4b) or in subsequent spatial coverage analysis, which relied on unambiguous trajectory assignment in accordance with known direction- and trajectory-dependence of hippocampal spatial firing[25,65–67]. Less stringent restriction of positional data produced qualitatively equivalent results.

For each unit, an occupancy-normalized firing map was calculated for each of the four task trajectories. First, total spike counts and occupancy durations were calculated for 2-cm spatial bins on each trajectory. Both the occupancy and spike counts per bin were smoothed with a Gaussian ($\sigma=4$ cm), then spike counts were divided by occupancy to produce the unit's smoothed occupancy-normalized firing map. The peak spatial firing rate was the maximum value in the occupancy-normalized map. A bin counted towards spatial coverage (Fig. 3b) if its occupancy-normalized rate was >2 Hz. Spatial coverage was quantified in each unit's highest mean firing rate task epoch. Seven units (CA1: 2 units, CA2 N: 5 units) were not included in spatial coverage quantification because of a failure of subjects to visit one of the maze arms in the units' highest firing rate task epochs. Quantification using additional velocity cutoffs and spatial firing thresholds is shown in Extended Data Fig. 4a.

Two-dimensional occupancy-normalized firing maps were constructed with 1-cm (W-maze) or 0.5-cm (rest environment) square bins. For example plots, these maps were smoothed with a symmetric 2D Gaussian ($\sigma=3$ cm for maze; $\sigma=1.5$ cm for rest environment); for nesting position analyses in the rest environment, no smoothing was performed. Data during SWR periods were excluded from all spatial firing plots and analyses.

Well firing. Well periods were defined as times when the subject's linear position matched that of the reward well (<2 cm separation). Well visits were defined as well periods that lasted at least 2 s and were preceded earlier in the recording epoch by a well period at a different well. In instances in which subjects re-visited the well they departed from before visiting another well, a well visit was only registered after an exclusion period of 5 s. Well entry times (designated $t=0$ in well raster plots) were defined as the beginning of well visits.

To calculate the well specificity index (WSI) of a unit, the well firing rate at each of the three wells of the task was first determined. Well firing rate was specifically calculated from the intersection of well periods with non-SWR immobility periods (well intersectional time). Next, each of the three well firing rates was divided by the numerical sum of the three well firing rates (normalization) to create a three-category (well A versus B versus C) probability distribution of firing activity. This probability distribution was subsequently treated as a circular distribution with a vector whose length corresponded to the probability mass for well A placed at 0°, a vector for well B at 120°, and a vector for well C at 240°. The magnitude of the vector sum (resultant), defined as the WSI, was used as a measure of well-specific firing. The WSI directly reflects specificity of firing: a WSI = 0 corresponds to equal firing at all three wells (completely non-specific), WSI = 0.5 corresponds to firing at two wells, and WSI = 1 corresponds to firing at one well.

The WSI was calculated in a unit's highest mean firing task epoch, and was only calculated when (i) at least 100 spikes were observed during well intersectional time, (ii) at least 5 s of well intersectional time was available for each of the three wells, (iii) the firing rate (during well intersectional time) for at least one well exceeded 0.5 Hz. These minimum activity criteria ensured that the WSI was calculated only for units that were unequivocally active at wells and for which adequate data at each well were available.

Theta analysis. To estimate theta phase, LFP from the REF tetrode (located in corpus callosum overlying right dorsal hippocampus[68]) was filtered at 5–11 Hz. The phase of the Hilbert transform of the filtered REF LFP was then designated as

© 2016 Macmillan Publishers Limited. All rights reserved

the theta phase[31,68]. For a given unit, theta phase locking analysis was performed for locomotor periods ($>4\,cm\,s^{-1}$) in task epochs, and moreover only when at least 50 spikes where present in these periods.

Spike- and SWR-triggered averaging of LFP (STA and RTA). Spike-triggered averages of LFP (STAs) were calculated for spiking in task epochs, moreover specifically for two distinct period types: locomotion and non-SWR immobility. For a given unit, STAs were calculated only when at least 100 spikes in the period type were observed. In each subject, the recording electrodes for each of four LFP reference regions (REF and CA2, CA3, and DG when available) were kept constant over all recording days. Each LFP recording site either reported principal units for its correspondent region (if CA2, CA3, DG) or was within 60 μm of the depth range at which principal units were detected, as determined from records of tetrode adjustment depths. In cases where the LFP reference region was the same as the region in which the unit was located, the parent electrode of the unit was chosen as the LFP reference.

For each unit for which an STA was calculated, a matched SWR-triggered average of LFP (RTA) was calculated, using the same LFP reference site and averaging across all SWRs detected in the same task recording epochs as the unit. RTAs were calculated by averaging LFP aligned to the time of peak power (designated $t=0$) in the multisite ripple band power (power at 150–250 Hz across CA1 sites, see above) for each SWR.

To evaluate the spectral components of the STAs and RTAs, the power spectral density (PSD) of individual unit STAs and RTAs (2-s LFP traces) was calculated using Welch's method (pwelch, Matlab Signal Processing Toolbox). Spectral analysis is shown for STAs/RTAs of LFP recorded in DG (Fig. 4d), as DG LFP showed the largest amplitude low-frequency signals.

N wave firing. To detect unit firing in association with the N wave, unit STAs were analysed. Specifically, unit STAs were classified into distinct groups using the following procedure. First, non-SWR immobility STAs and RTAs were calculated from LFP filtered at 1–4 Hz. Since the N wave as originally identified (Fig. 4c) was largest at DG, then CA3, and then CA2, the STAs were calculated for LFP at DG sites when available, then at CA3 when available, then at CA2. Furthermore, for an LFP recording site to be used to calculate classifiable STAs, the RTA at that site had to be significantly negative at $t=0$ ($P<0.001$ level, signed-rank). In a small number of cases in which this condition was not satisfied, LFP from the next available region, if available, was used. Thus SWR sharp waves were verified to manifest as negative deflections at recording sites used to calculate STAs.

A unit STA was classified in two specific cases: (1) when the STA at the time of spiking ($t=0$) was positive and the nearest local extremum was a maximum (peak), and (2) when the STA at the time of spiking was negative and nearest local extremum was a minimum (trough). A small number of units showing positive troughs or negative peaks were left unclassified (CA1: 10 out of 146 units, CA2 N units: 1 out of 58 units, CA3: 3 out of 137 units, interneurons: 10 out of 63 units, plotted at bottom in Extended Data Figs 7b, 7d and 8a). Units satisfying (1) and (2) are referred to as 'positive STA' and 'negative STA' unit populations, respectively. Units satisfying (1) were identified as firing in association with the N wave (N wave-coupled).

Sleep state identification. In rest epochs, awake periods were identified as times in which head speed was $>4\,cm\,s^{-1}$ in addition to times $<4\,cm\,s^{-1}$ within 7 s of a previous movement $>4\,cm\,s^{-1}$. Thus, given the behavioural state criteria (see above), for each distinct period in which a subject stopped moving, no more than 5 s were included as awake immobility.

Candidate sleep periods were identified as times $<4\,cm\,s^{-1}$ preceded by 60 s with no movement $>4\,cm\,s^{-1}$. REM periods within candidate sleep times were identified following an established procedure[69]. Specifically, the ratio of Hilbert amplitudes (smoothed with a Gaussian kernel, $\sigma=1$ s) of theta (5–11 Hz) to delta (1–4 Hz) filtered LFP was calculated for all available CA1 tetrodes (referenced to cerebellar ground), and the mean taken over tetrodes. For each rest epoch, a threshold (range: 1.2–1.8) was manually set to capture sustained periods (10 s minimum duration) in which the theta:delta ratio was elevated. LFP and position data from each detected REM period were visually inspected.

For a given day's set of candidate sleep times outside of REM periods, LFP from each available CA1, CA3, and DG recording site was squared then smoothed with a Gaussian kernel ($\sigma=300$ ms). The square root of the smoothed signal was then z-scored and summed across sites. The sum trace was in turn z-scored to obtain an aggregate hippocampal LFP amplitude. For each rest epoch, the distribution of aggregate LFP amplitudes was plotted (example trace and distribution in Fig. 5a). From a rest epoch in which bimodality was observed, the value at the local minimum separating the two modes was chosen as the SIA z-score threshold for the day. SIA periods were defined as non-REM times in which the aggregate LFP amplitude was below the threshold, and LIA periods otherwise. In a minority of cases, a threshold was chosen to isolate a heavy left tail of the distribution, later verified in the LFP to correspond to SIA periods. Across all recording days ($n=73$ days) the SIA threshold was -0.67 ± 0.24 (z-score, mean ± s.d.), and median period durations were SIA: 1.20 s; LIA: 2.48 s; REM: 27 s. Visual inspection of LFPs confirmed that SIA periods could often be ~1 s in duration[33], indicating rapid switching between distinct sleep states (Fig. 5a, b). Also, as previously reported[33], slight movements without overt awaking could at times observed during SIA (Fig. 5b). Lastly, though SWRs in sleep typically occurred during LIA, SWRs at times occurred within identified SIA periods[33]. Thus, to isolate SIA periods optimally, SWR periods were not included in calculations referencing SIA periods.

Sleep periods were candidate sleep periods at least 90 s in duration and containing extended (>5 s) continuous LIA periods. Across all recording days, 465 sleep periods (median duration: 218 s) were identified.

Nesting position coding. Unit firing rates during SIA were calculated for individual sleep periods. Sleep periods in which a unit's SIA firing rate was >2 Hz were categorized as SIA ON for the unit, and SIA OFF otherwise. Next, the 2D spatial firing map (non-smoothed, see above) for the unit from awake periods in the same ~20-min rest epoch was referenced. During awake periods, the total number of spikes and total time spent at positions >5 cm from the subject's head position at the beginning of the sleep period (nesting position) were categorized as Nest OUT, and likewise Nest IN for positions <5 cm. If there were additional sleep periods of a given type (SIA ON or SIA OFF) available for a unit, then the spike counts and durations spent were summed within the Nest OUT/IN categories for the respective nesting positions of the additional sleep periods. Firing rate for a given category (for example, SIA ON, Nest OUT) was calculated as the total number of spikes divided by the total time.

A unit coding for nesting position is expected to show two firing patterns (dual criteria): if classified as SIA ON in a given sleep period, the unit is expected to show higher firing rates, during awake periods, at positions nearer to the nesting position (Nest IN, <5 cm) corresponding to the sleep period; conversely, if classified as SIA OFF in a given sleep period, the unit is expected to show higher firing rates, during awake periods, at positions farther from the nesting position (Nest OUT, >5 cm) corresponding to the sleep period.

Unit populations were tested for nesting position coding with two approaches. In the first, absolute firing rates were compared between Nest IN versus OUT periods for both SIA ON and SIA OFF groups[33] (Extended Data Fig. 10j). In the second (Fig. 5f), firing rates in the Nest IN versus Nest OUT conditions were compared for each unit by calculating a measure termed the nesting position specificity index, calculated as $2\times fr_{IN}/(fr_{IN}+fr_{OUT})-1$. Using this measure, a firing rate in Nest IN that is twice as high as in Nest OUT yields a value of 1/3; three times as high yields a value of 1/2.

For either the absolute firing rate or the specificity index approach, the dual criteria for nesting position coding in a unit population were (1) higher firing during Nest IN versus Nest OUT for the SIA ON group and (2) higher firing during Nest OUT versus Nest IN for the SIA OFF group.

Statistics. All statistical tests were two-sided.

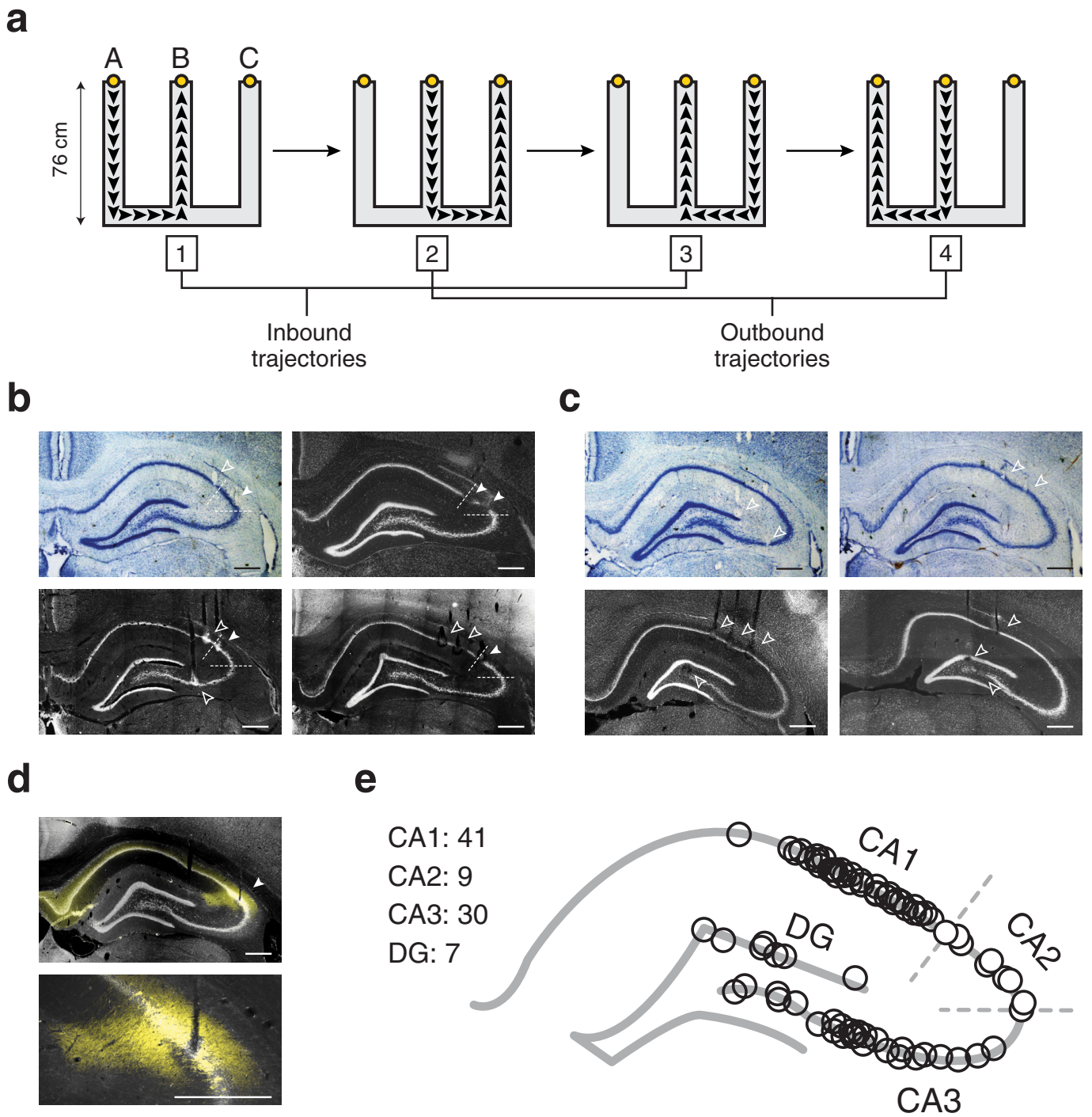
Code availability. All custom-written code is available upon request.

51. Gray, C. M., Maldonado, P. E., Wilson, M. & McNaughton, B. Tetrodes markedly improve the reliability and yield of multiple single-unit isolation from multi-unit recordings in cat striate cortex. *J. Neurosci. Methods* **63,** 43–54 (1995).
52. Potter, G. B., *et al.* Generation of Cre-transgenic mice using *Dlx1/Dlx2* enhancers and their characterization in GABAergic interneurons. *Mol. Cell Neurosci.* **40,** 167–186 (2009).
53. Neunuebel, J. P. & Knierim, J. J. Spatial firing correlates of physiologically distinct cell types of the rat dentate gyrus. *J. Neurosci.* **32,** 3848–3858 (2012).
54. Ishizuka, N., Cowan, W. M. & Amaral, D. G. A quantitative analysis of the dendritic organization of pyramidal cells in the rat hippocampus. *J. Comp. Neurol.* **362,** 17–45 (1995).
55. Woodhams, P. L., Celio, M. R., Ulfig, N. & Witter, M. P. Morphological and functional correlates of borders in the entorhinal cortex and hippocampus. *Hippocampus* **3,** 303–311 (1993).
56. Amaral, D. G. & Lavenex, P. in *The Hippocampus Book* (eds Andersen, P. et al.) 37–114 (Oxford Univ. Press, 2007).
57. Cui, Z., Gerfen, C. R. & Young, W. S., III. Hypothalamic and other connections with dorsal CA2 area of the mouse hippocampus. *J. Comp. Neurol.* **521,** 1844–1866 (2013).
58. Csicsvari, J., Hirase, H., Czurko, A., Mamiya, A. & Buzsaki, G. Fast network oscillations in the hippocampal CA1 region of the behaving rat. *J. Neurosci.* **19,** RC20 (1999).
59. Ranck, J. B. Jr. Studies on single neurons in dorsal hippocampal formation and septum in unrestrained rats. I. Behavioral correlates and firing repertoires. *Exp. Neurol.* **41,** 462–531 (1973).
60. Fox, S. E. & Ranck, J. B. Jr. Electrophysiological characteristics of hippocampal complex-spike cells and theta cells. *Exp. Brain Res.* **41,** 399–410 (1981).
61. Skaggs, W. E. & McNaughton, B. L. Replay of neuronal firing sequences in rat hippocampus during sleep following spatial experience. *Science* **271,** 1870–1873 (1996).

© 2016 Macmillan Publishers Limited. All rights reserved

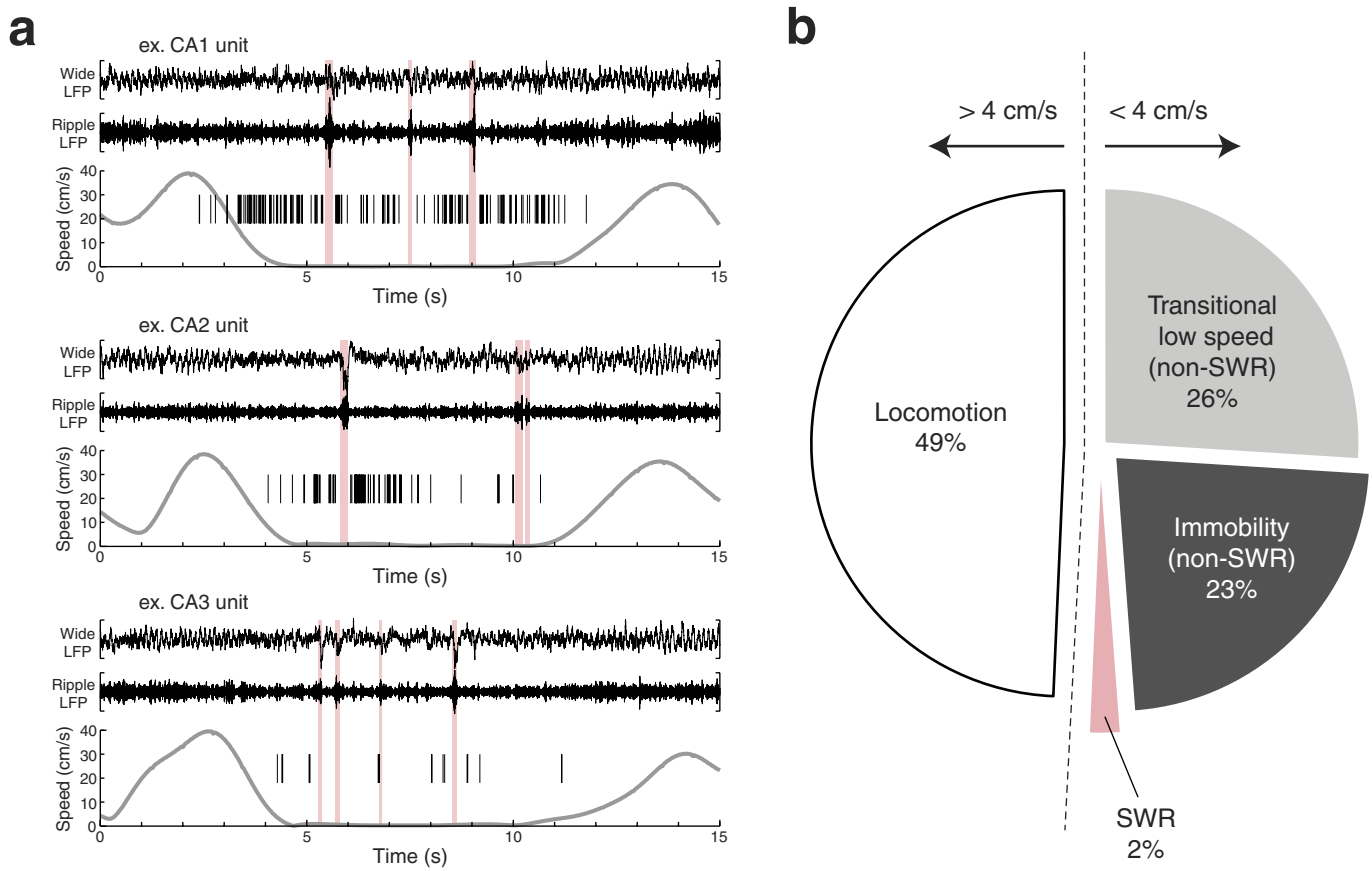
62. Csicsvari, J., Hirase, H., Czurko, A., Mamiya, A. & Buzsaki, G. Oscillatory coupling of hippocampal pyramidal cells and interneurons in the behaving rat. *J. Neurosci.* **19,** 274–287 (1999).
63. Kemere, C., Carr, M. F., Karlsson, M. P. & Frank, L. M. Rapid and continuous modulation of hippocampal network state during exploration of new places. *PLoS ONE* **8,** e73114 (2013).
64. Chen, Z., Resnik, E., McFarland, J. M., Sakmann, B. & Mehta, M. R. Speed controls the amplitude and timing of the hippocampal gamma rhythm. *PLoS ONE* **6,** e21408 (2011).
65. Frank, L. M., Brown, E. N. & Wilson, M. Trajectory encoding in the hippocampus and entorhinal cortex. *Neuron* **27,** 169–178 (2000).
66. Wood, E. R., Dudchenko, P. A., Robitsek, R. J. & Eichenbaum, H. Hippocampal neurons encode information about different types of memory episodes occurring in the same location. *Neuron* **27,** 623–633 (2000).
67. Ito, H. T., Zhang, S. J., Witter, M. P., Moser, E. I. & Moser, M. B. A prefrontal-thalamo-hippocampal circuit for goal-directed spatial navigation. *Nature* **522,** 50–55 (2015).
68. Lubenov, E. V. & Siapas, A. G. Hippocampal theta oscillations are travelling waves. *Nature* **459,** 534–539 (2009).
69. Mizuseki, K., Diba, K., Pastalkova, E. & Buzsaki, G. Hippocampal CA1 pyramidal cells form functionally distinct sublayers. *Nature Neurosci.* **14,** 1174–1181 (2011).
70. Jadhav, S. P., Kemere, C., German, P. W. & Frank, L. M. Awake hippocampal sharp-wave ripples support spatial memory. *Science* **336,** 1454–1458 (2012).
71. Lee, S. E. *et al.* RGS14 is a natural suppressor of both synaptic plasticity in CA2 neurons and hippocampal-based learning and memory. *Proc. Natl Acad. Sci. USA* **107,** 16994–16998 (2010).
72. Suzuki, S. S. & Smith, G. K. Spontaneous EEG spikes in the normal hippocampus. I. Behavioral correlates, laminar profiles and bilateral synchrony. *Electroencephalogr. Clin. Neurophysiol.* **67,** 348–359 (1987).
73. Buzsáki, G. Two-stage model of memory trace formation: a role for "noisy" brain states. *Neuroscience* **31,** 551–570 (1989).
74. Harris, K. D., Hirase, H., Leinekugel, X., Henze, D. A. & Buzsaki, G. Temporal interaction between single spikes and complex spike bursts in hippocampal pyramidal cells. *Neuron* **32,** 141–149 (2001).
75. Mizuseki, K., Royer, S., Diba, K. & Buzsaki, G. Activity dynamics and behavioral correlates of CA3 and CA1 hippocampal pyramidal neurons. *Hippocampus* **22,** 1659–1680 (2012).
76. Harvey, C. D., Collman, F., Dombeck, D. A. & Tank, D. W. Intracellular dynamics of hippocampal place cells during virtual navigation. *Nature* **461,** 941–946 (2009).
77. Epsztein, J., Brecht, M. & Lee, A. K. Intracellular determinants of hippocampal CA1 place and silent cell activity in a novel environment. *Neuron* **70,** 109–120 (2011).
78. Grienberger, C., Chen, X. & Konnerth, A. NMDA receptor-dependent multidendrite Ca(2+) spikes required for hippocampal burst firing *in vivo*. *Neuron* **81,** 1274–1281 (2014).
79. Bittner, K. C. *et al.* Conjunctive input processing drives feature selectivity in hippocampal CA1 neurons. *Nature Neurosci.* **18,** 1133–1142 (2015).
80. Klausberger, T. & Somogyi, P. Neuronal diversity and temporal dynamics: the unity of hippocampal circuit operations. *Science* **321,** 53–57 (2008).
81. Diba, K., Amarasingham, A., Mizuseki, K. & Buzsaki, G. Millisecond timescale synchrony among hippocampal neurons. *J. Neurosci.* **34,** 14984–14994 (2014).
82. Royer, S. *et al.* Control of timing, rate and bursts of hippocampal place cells by dendritic and somatic inhibition. *Nature Neurosci.* **15,** 769–775 (2012).
83. Skaggs, W. E., McNaughton, B. L., Gothard, K. & Markus, E. in *Advanced in Neural Information Processing Systems* (eds Hanson, S., Cowan, J. D. & Giles, C. L.) 1030–1037 (Morgan Kaufmann, 1993).

© 2016 Macmillan Publishers Limited. All rights reserved



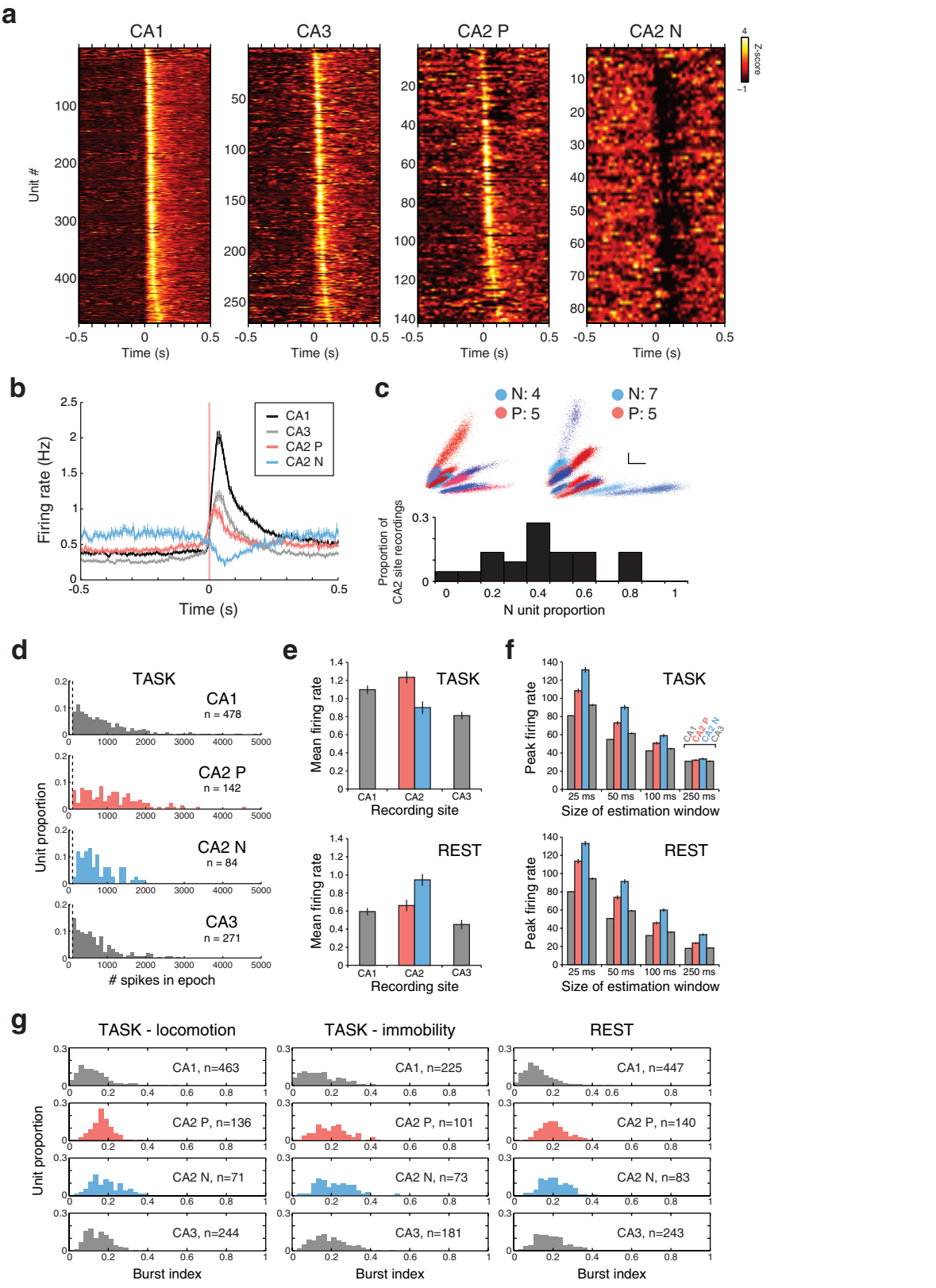
Extended Data Figure 1 | Behavioural task and hippocampal recording sites. a, Continuous spatial alternation task[21,24,65,70]. The task environment is a W-shaped maze with a centre arm and two outer arms. Reward (~0.3 ml of sweetened evaporated milk) is dispensed through 3-cm diameter wells (yellow circles; designated 'A', 'B', and 'C' for reference in data plots), located at the end of each arm. Rats are rewarded for performing the trajectory sequence shown (numbered 1–4), in which the correct destination after visiting the centre well is the less recently visited outer well. All subjects stopped locomoting upon reaching the reward wells to check for (by licking) and consume reward. Subjects also stopped intermittently elsewhere in the maze (most frequently at maze junctions), particularly in earlier exposures to the task. **b**, **c**, Example hippocampal histological sections showing tetrode tracks and electrolytic lesions in CA1, CA2, CA3, and DG. Nissl-stained sections show neuronal cell bodies in dark blue, while sections stained with Neurotrace show neuronal cell bodies in light grey. Panel **b** shows example sections with sites overlapping with the CA2 cytoarchitectural locus[28–30,36,47,50,54–57] (enclosed by dotted lines; characterized by dispersion of the hippocampal cell layer in the region between CA1 and CA3). Filled arrowheads indicate sites overlapping with CA2, while empty arrowheads indicate non-CA2 recording sites. The CA2 site assignment was deliberately inclusive to maximize detection of units at CA2 with novel physiological responses (N units, Fig. 1 and Extended Data Fig. 3). Scale bars: 500 μm. **d**, Coronal hippocampal section stained with a neuronal cell body marker (light grey; NeuroTrace) and CA2 marker (yellow; RGS14[36,47,71]). Bottom, magnified view of a track left by a CA2 site tetrode. Scale bars: 500 μm. **e**, Survey of recording sites included in the study data set. Diagrammed in a representative hippocampal section are recording site locations (circles) of seven subjects from which coronal hippocampal sections were taken (CA1: 41 sites, CA2: 9 sites, CA3: 30 sites, DG: 7 sites; two additional CA2 sites near the septal pole of hippocampus not shown). Dotted lines enclose the CA2 anatomical locus, with overlapping recording sites shown as filled circles. The majority of CA1 recordings were in CA1c, while the majority of CA3 recordings were in CA3b.

© 2016 Macmillan Publishers Limited. All rights reserved



Extended Data Figure 2 | Observation of firing during immobility. **a**, Non-SWR immobility firing in three example principal units recorded in CA1, CA2, and CA3. Each firing raster is shown as vertical lines overlaid on a plot of the subject's head speed (grey trace). Top traces: wide-band LFP (0.5–400 Hz, scale bar: 800 μV) and ripple-band LFP (150–250 Hz, scale bar: 100 μV) traces from a simultaneous recording in CA1, to show hippocampal network state. SWR periods are plotted as pink zones. Note that substantial firing occurs in the absence of (i) locomotion, (ii) detectable SWRs, and (iii) detectable theta (regular ~8 Hz rhythm visible in the LFP during moving periods). **b**, Proportions of time spent in different period types over all task recording epochs ($n = 222$ task recording epochs, 8 subjects) in the data set. During the performance of the task, a substantial proportion of time was spent at low speeds and immobility, moreover when SWRs were not detected. Transitional low speed periods were times when the subject's speed was $< 4\,\mathrm{cm\,s^{-1}}$ and within 2 s (earlier or later) of periods of movement $> 4\,\mathrm{cm\,s^{-1}}$, while immobility periods were times when the speed was $< 4\,\mathrm{cm\,s^{-1}}$ and separated more than 2 s (earlier or later) from periods of movement $> 4\,\mathrm{cm\,s^{-1}}$. Note that SWR periods comprised only a minority of time spent at low speeds, consistent with past observations[17,72,73].

© 2016 Macmillan Publishers Limited. All rights reserved

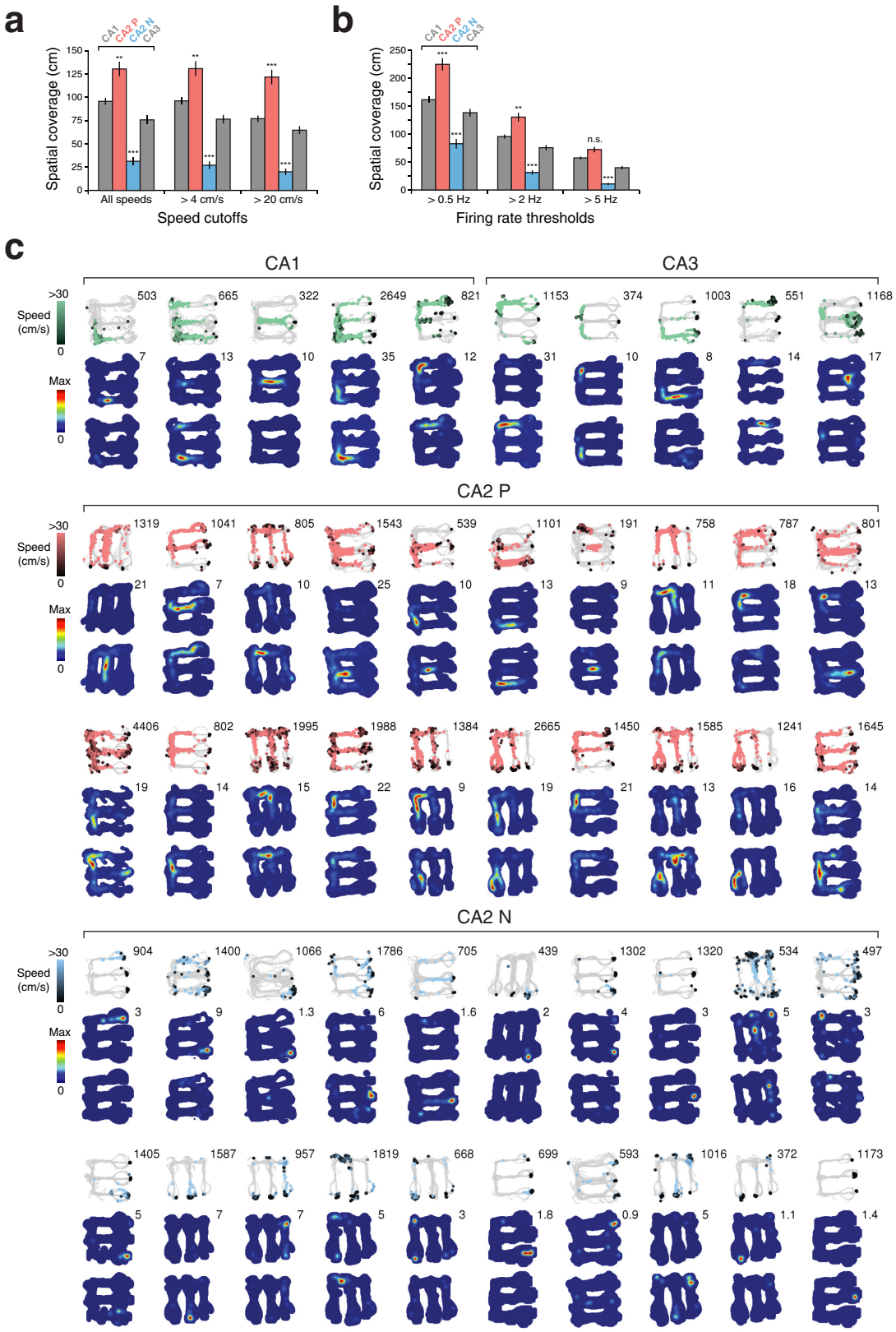


Extended Data Figure 3 | See next page for caption.

© 2016 Macmillan Publishers Limited. All rights reserved

Extended Data Figure 3 | Firing properties of CA1, CA2, and CA3 units. a, Peri-SWR time histograms (PSTHs; SWR onset at $t = 0$) of firing for all principal units in the task unit set. SWRs from both task and rest epochs were used to calculate PSTHs (1-ms bins), which were smoothed with a Gaussian kernel ($\sigma = 10$ ms). Each unit's mean PSTH was then z-scored (colour bar) and plotted in a row. Units are sorted by the time of the maximum z-scored rate from 0 to +100 ms. **b**, PSTHs for the four hippocampal unit populations (mean ± s.e.m.; number of units: CA1: 478 units; CA3: 271; CA2 P: 142; CA2 N: 84) analysed in this study. Using formal criteria (described in Methods), units that were inhibited during SWRs constituted a majority subset (56 of 84) of N units, and were observed in every subject with CA2 site recordings (5 subjects, inhibition apparent in examples in Fig. 1d and N unit PSTHs in **a**). Here, the reduction of firing in these neurons manifests in the N unit population response as a dip in firing rate at the time of SWRs (N unit population in blue), in contrast to the CA1, CA3, and CA2 P unit populations, all of which showed sharp increases in firing during SWRs[19]. Time bins: 5 ms. **c**, Proportion of N units in CA2 site recordings. Upper plots: spike amplitudes measured on two channels of a tetrode for two example CA2 site recordings (left and right). Colours indicate spikes of N (blue-based tones) and P (red-based tones) units. The number of well-isolated principal units of each type is reported at upper right. Scale bars (x and y), 100 μV. Lower plot: proportion of N units across CA2 site recordings with at least four clustered putative principal units. CA2 recording sites typically reported N and P units concurrently, indicating that the spiking of two distinct hippocampal principal cell types was detectable at a single CA2 recording site. **d**, Unit spike counts in 15-min task epochs for each principal unit population. The counts were taken from each unit's highest mean rate task epoch. Spikes that occurred during SWR periods were not included in these counts. **e**, Mean firing rate for each principal unit population (mean ± s.e.m.). The mean rates were calculated from the highest rate epoch for each unit, either among task (top, TASK) or rest (bottom, REST) epochs. TASK number units (task unit set): CA1: 478 units; CA2 P: 142; CA2 N: 84; CA3: 271. REST number units (subset of task unit set with available rest epoch data): CA1: 454 units; CA2 P: 142; CA2 N: 84; CA3: 252. All spikes and epoch times were included. **f**, Peak firing rate for each principal unit population (mean ± s.e.m.). The peak rates were estimated from the highest rate epochs for each unit, either among task (top, TASK) or rest (bottom, REST) epochs. The peak rate was the maximum instantaneous firing rate (IFR) exhibited by the unit. Here, the IFR was estimated by convolving each unit's spike train (1-ms bins) with Gaussian kernels of different sizes (x-axis, times refer to s.d. of the kernel). TASK number units (task unit set): CA1: 478 units; CA2 P: 142; CA2 N: 84; CA3: 271. REST number units (subset of task unit set with available rest epoch data and at least 100 spikes in a rest epoch): CA1: 421, CA2 P: 138, CA2 N: 82, CA3: 197 units. All spikes and epoch times were included. **g**, Burst firing in each principal unit population. The burst index of a unit was defined as the proportion of inter-spike intervals (ISI) less than 6 ms[74,75]. Burst indices were calculated separately for three conditions: locomotion (left panels) and immobility (centre) in task epochs, and also for rest epochs (right). In a given condition, a minimum of 100 spikes was required for a unit to be analysed. Moreover, for locomotor and immobility periods from task epochs, only ISIs of spikes that were successive within single uninterrupted periods of a given type were included. Lastly, in this analysis, SWR periods were not excluded. Notably, CA2 N units showed high levels of bursting, suggesting that these units correspond to hippocampal principal (pyramidal) neurons[59,60,62,76–79].

© 2016 Macmillan Publishers Limited. All rights reserved

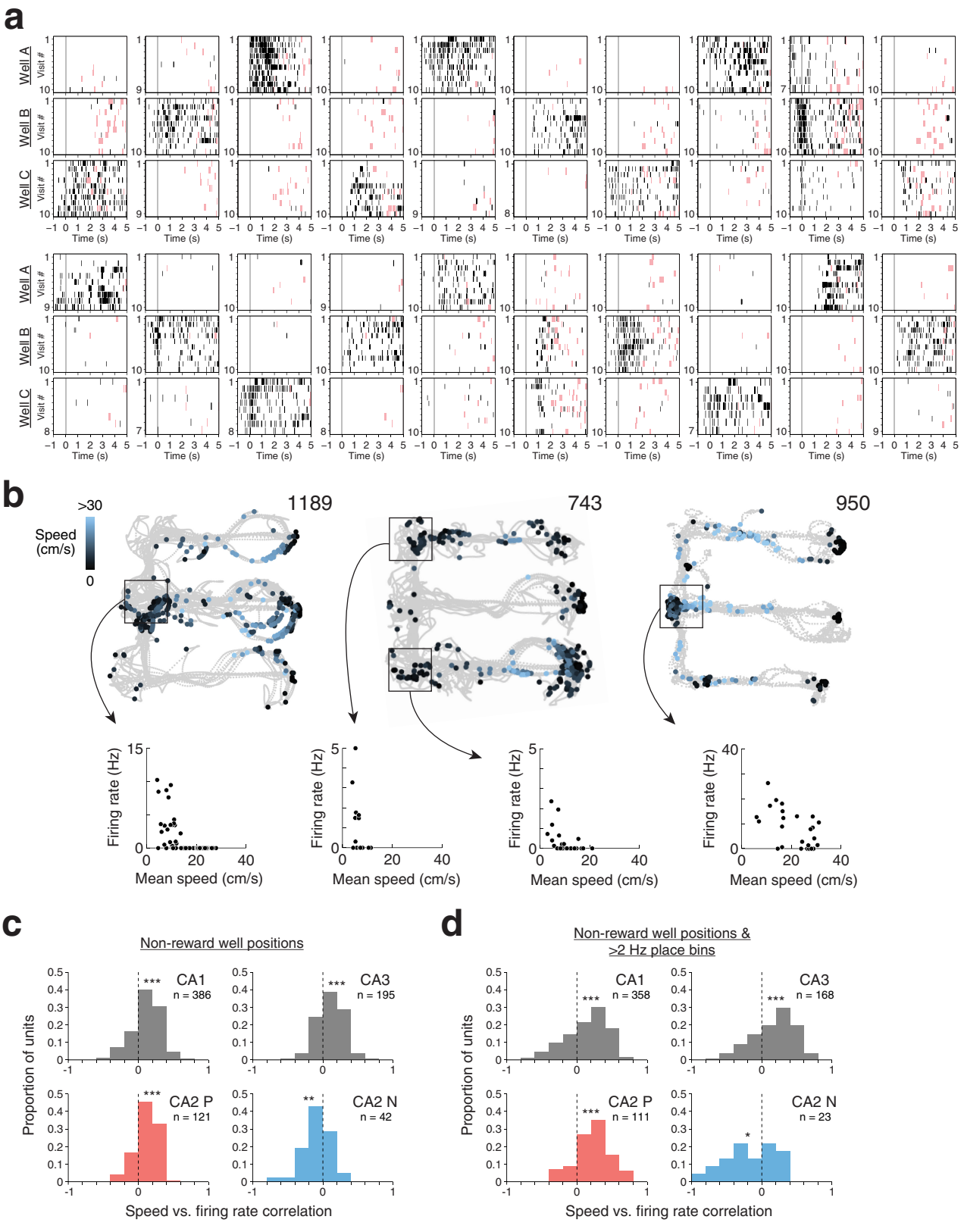


Extended Data Figure 4 | See next page for caption.

© 2016 Macmillan Publishers Limited. All rights reserved

Extended Data Figure 4 | Spatial firing of CA1, CA2, and CA3 units. For the analyses in **a** and **b**, unit sample sizes are the same as in Fig. 3b. **a**, Spatial coverage at different speed cutoffs (mean ± s.e.m.), in which only data from periods satisfying the speed condition were analysed. For each speed cutoff, a firing rate threshold of 2 Hz was used. The all speeds condition is the same as in Fig. 3b. CA2 $P >$ each other unit population, Kruskal–Wallis ANOVA, Tukey's post hoc tests, $P = 0.0015$ for all speeds, $P = 0.0021$ for >4 cm s^{-1}, and $P < 10^{-5}$ for >20 cm s^{-1}. CA2 $N <$ each other unit population, Kruskal–Wallis ANOVA, Tukey's post hoc tests, $P < 10^{-6}$ for all speeds, $P < 10^{-7}$ for >4 cm s^{-1}, and $P < 10^{-8}$ for >20 cm s^{-1}. $^{**}P < 0.01$; $^{***}P < 0.001$. **b**, Spatial coverage at different firing rate thresholds (mean ± s.e.m.). For each threshold level, spikes at all speeds were analysed. CA2 $P >$ each other unit population, Kruskal–Wallis ANOVA, Tukey's post hoc tests, $P < 10^{-5}$ for >0.5 Hz, $P = 0.0015$ for >2 Hz, and $P = 0.11$ for >5 Hz. CA2 $N <$ each other unit population, Kruskal–Wallis ANOVA, Tukey's post hoc tests, $P < 10^{-4}$ for >0.5 Hz, $P < 10^{-6}$ for >2 Hz, and $P < 10^{-7}$ for >5 Hz. $^{**}P < 0.01$; $^{***}P < 0.001$, n.s., not significant at $P < 0.05$. **c**, Example spatial firing maps for CA1, CA3, CA2 P, and CA2 N units. Each column corresponds to data from an individual unit from a single 15-min task epoch. Upper row: raw maps showing positions visited by the subject (grey) and positions where the unit fired (coloured opaque points, plotted chronologically and with darker colour values at lower speeds). The total number of spikes (outside of SWR periods) in the epoch is reported at upper right. Lower two rows: occupancy-normalized firing maps, with the first row showing maps generated from data from outbound trajectories (centre to left or right arms) and the second row inbound trajectories (left or right to centre arm; Extended Data Fig. 1a). The spatial peak firing rate (highest rate for a occupancy-normalized bin) is shown at upper right. Shown are data from each unit's highest mean firing rate task epoch. Data from SWR periods were excluded from all plots. Notably, N units could show substantial firing at locations distinct from the reward wells (N unit examples with spike counts of 534, 497, 957, 1819, 668, 1,016 and 372).

© 2016 Macmillan Publishers Limited. All rights reserved

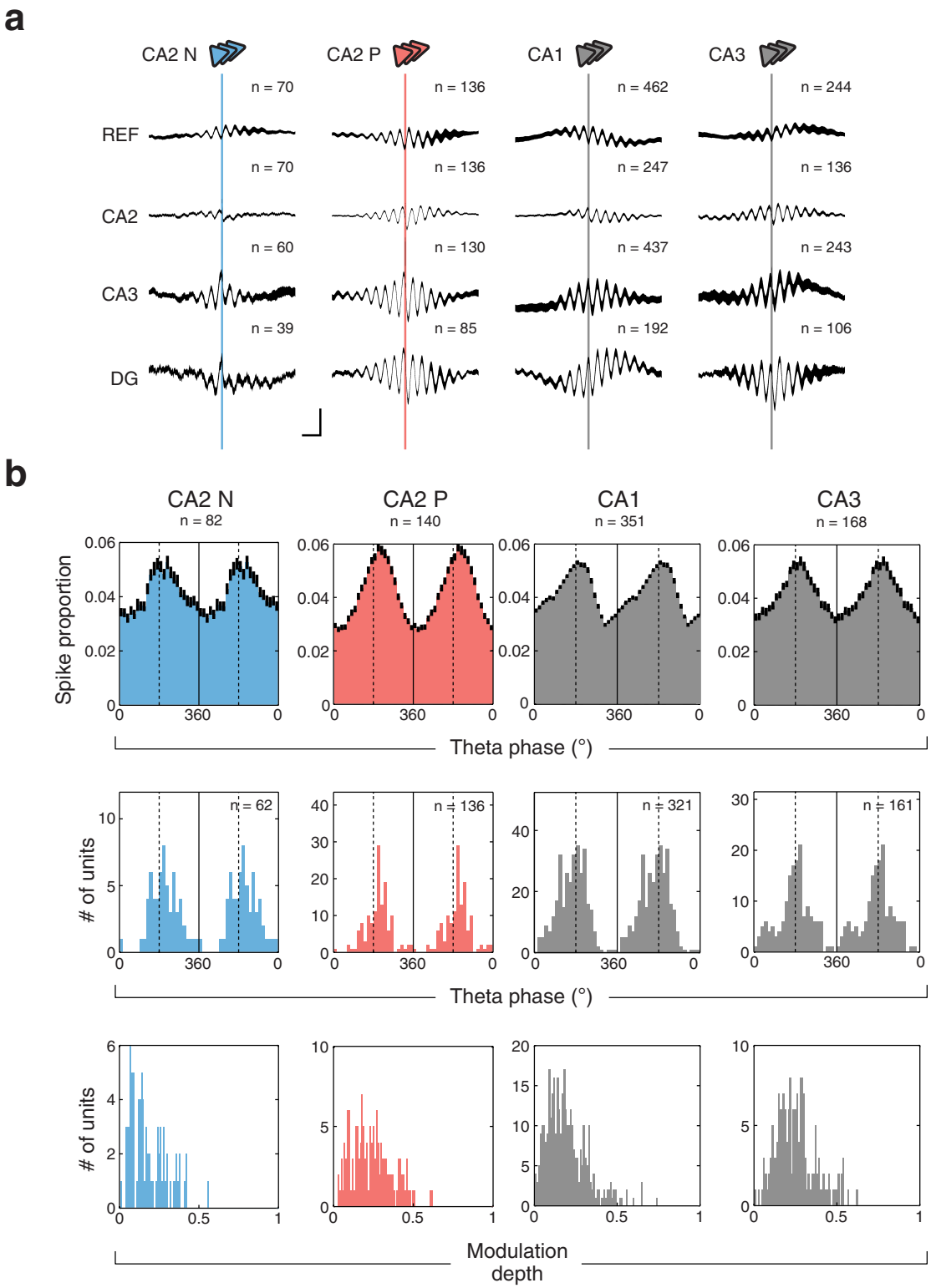


Extended Data Figure 5 | See next page for caption.

© 2016 Macmillan Publishers Limited. All rights reserved

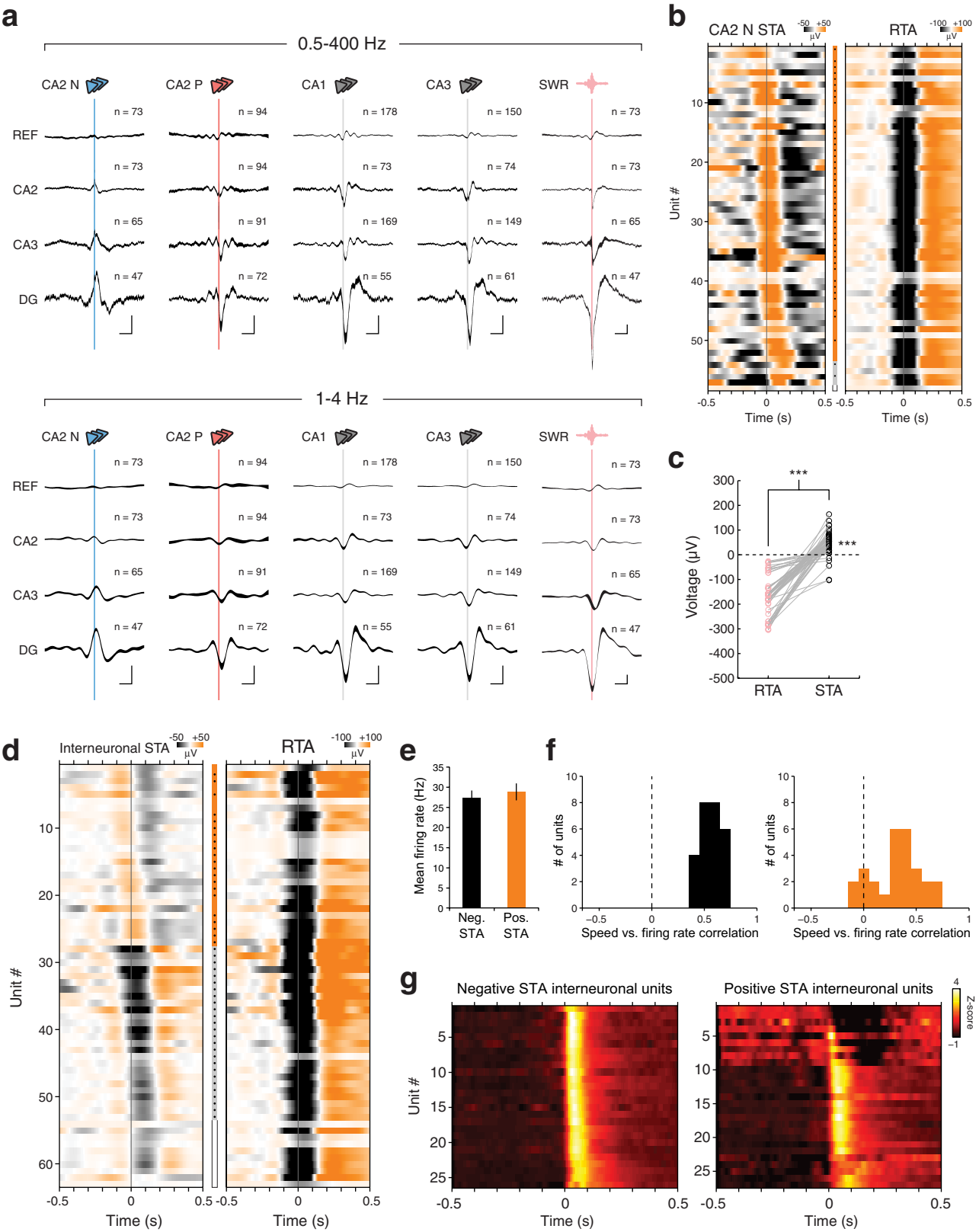
Extended Data Figure 5 | N unit spatial coding. a, Reward well firing rasters of 20 example N units. For each unit, data from the final ten (if available) entries of the subject's head into each of the three task reward wells (A, B, C) from a single task epoch are shown. The time of well entry ($t = 0$) is plotted as a grey line. SWR periods are plotted in the background as pink zones. Note that firing for a given N unit was typically specific to one of the three reward wells. **b**, Non-reward well firing in three example N units. The rightmost example is the same as the third example in Fig. 2a. Upper row: spatial firing maps. Locations visited by the subject are plotted in grey, while locations at which the unit fired are plotted as coloured opaque points (in blue) plotted chronologically and with darker colour values at lower speeds. Total spike counts are indicated at upper right. In the task (Methods and Extended Data Fig. 1a), reward was delivered to the subjects only at the ends of the maze arms, thus locations elsewhere in the maze were not directly associated with reward. Lower row: firing rate versus speed of distinct visits to specific maze junctions (indicated with a square on spatial firing maps). Junction visits were identified as periods during which the subject's linear position (Methods) was within 10 cm of a maze junction. Firing rate was the total number of spikes divided by the visit duration. Mean speed was the average instantaneous head speed during the visit. To limit analysis to discrete traversals through a junction, visits that were both less than 1 s in duration and also had mean speeds $<10\,\mathrm{cm\,s^{-1}}$ were disregarded. Note that N units tended to fire at lower speed junction visits, and that some junction visits at higher speeds elicited no firing. **c**, Firing rate dependence on speed at non-reward task locations. Distribution of correlations (Pearson's r) between firing rate and log speed for each unit population. This analysis is the same as in Fig. 2b, except restricted to periods when the subject was located >30 cm from reward wells, moreover including only units that fired at least 50 spikes at these locations (outside of SWR periods). As in the location-inclusive case (Fig. 2b), the N unit population uniquely showed an anti-correlation ($r < 0$) of firing rate with speed. Pearson's r, mean ± s.d.; CA1: 0.12 ± 0.20, CA1 versus 0, $P < 10^{-23}$, signed-rank; CA3: 0.11 ± 0.18, CA3 versus 0, $P < 10^{-13}$, signed-rank; CA2 P: 0.12 ± 0.16, CA2 P versus 0, $P < 10^{-10}$, signed-rank; CA2 N: -0.09 ± 0.20, CA2 N versus 0, $P = 0.0056$, signed-rank; CA2 N versus CA2 P, $P < 10^{-8}$, rank-sum. Only units with significant correlations ($P < 0.05$) were included (CA1: 386/393 units, CA3: 195/196 units, CA2 P: 121/121 units, CA2 N: 42/42 units). $^{**}P < 0.01$; $^{***}P < 0.001$. **d**, Same analysis as **c**, except with an additional restriction to periods when the subject was located in linear positions where a unit had occupancy-normalized spatial coverage >2 Hz. Pearson's r, mean ± s.d.; CA1: 0.14 ± 0.30, CA1 versus 0, $P < 10^{-16}$, signed-rank; CA3: 0.17 ± 0.30, CA3 versus 0, $P < 10^{-10}$, signed-rank; CA2 P: 0.22 ± 0.23, CA2 P versus 0, $P < 10^{-12}$, signed-rank; CA2 N: -0.17 ± 0.33, CA2 N versus 0, $P = 0.031$, signed-rank; CA2 N versus CA2 P, $P < 10^{-6}$, rank-sum. Only units with significant correlations ($P < 0.05$) were included (CA1: 358/364 units, CA3: 168/168 units, CA2 P: 111/111 units, CA2 N: 23/24 units). $^{*}P < 0.05$; $^{***}P < 0.001$.

© 2016 Macmillan Publishers Limited. All rights reserved



Extended Data Figure 6 | Locomotor STAs and theta analysis. Unit spiking at speeds $> 4\,cm\,s^{-1}$ was analysed. **a**, Locomotor STAs. Plotted are mean STAs of hippocampal LFP for each principal unit population. LFP from four distinct recording sites (REF, CA2, CA3, DG) are plotted in rows. Vertical lines correspond to the time of spiking. The width of the trace indicates ± s.e.m. across individual unit STAs. The total trace length is 2 s. REF: reference electrode located in corpus callosum overlying dorsal hippocampus, reporting signals relative to a cerebellar ground screw. Scale bars, *x*, 250 ms; *y*, 50 μV. **b**, Theta phase locking analysis of each principal unit population. For comparison of theta phase preferences between unit populations in simultaneously recorded data, analysis was restricted to subjects in which all four unit types (CA1, CA3, CA2 N and CA2 P) were recorded. First row: mean circular distribution of spikes for each unit population. Error bars: ± s.e.m. across individual units. Second row: the distribution of mean circular phases for significantly modulated units ($P < 0.05$, Rayleigh tests, total number of significant units reported at upper right). Bottom row: the distribution of modulation depths (resultant length) for all units. In plots with theta phase (bin size: 15°; troughs at 180°, indicated in dotted lines), two cycles are shown to aid visual comparison. Surprisingly, we did not observe a ~90° phase lead of CA3 relative to CA1 as reported in a previous study[31], perhaps due to differences in CA3 recording locations.

© 2016 Macmillan Publishers Limited. All rights reserved

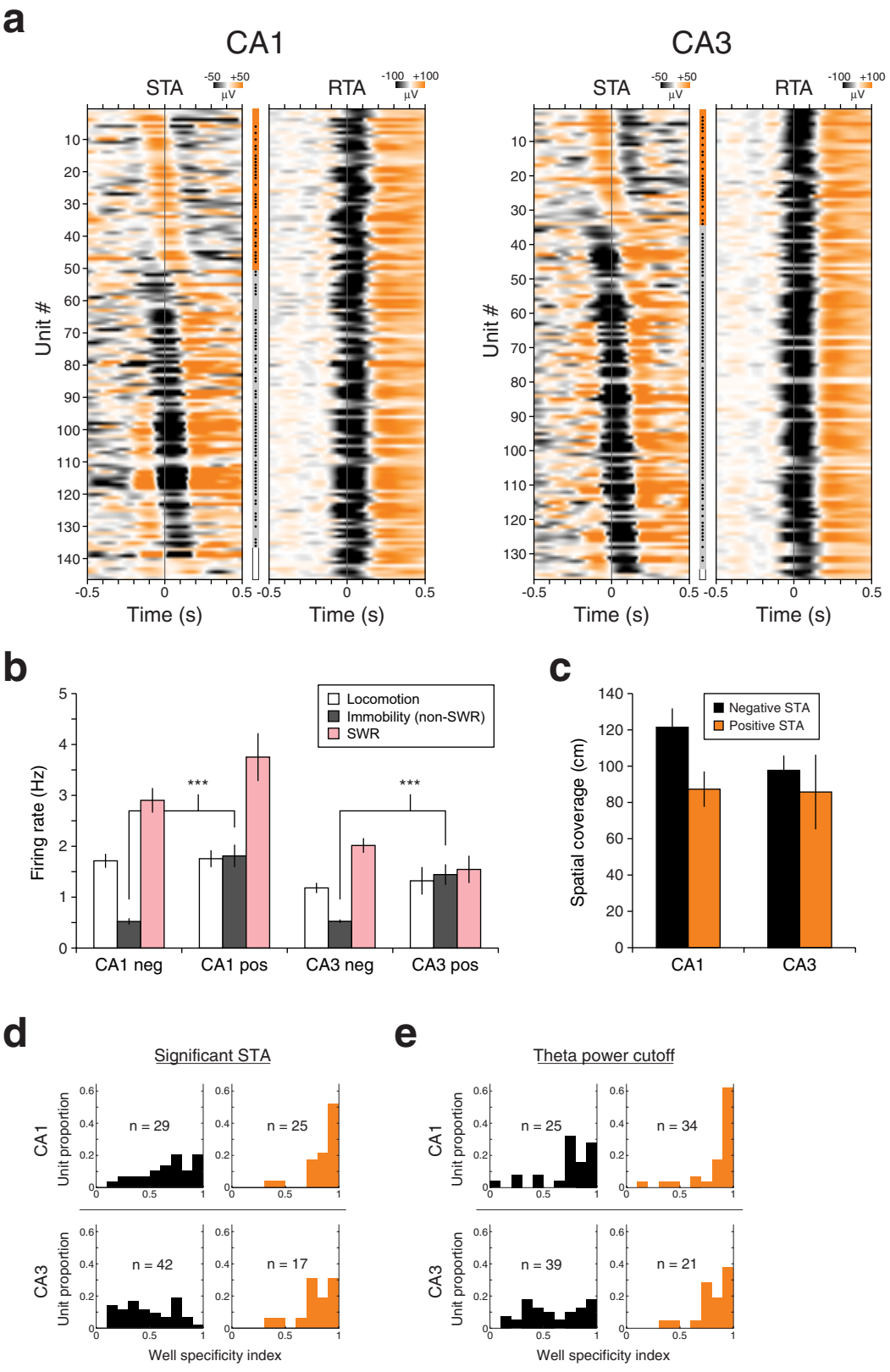


Extended Data Figure 7 | See next page for caption.

© 2016 Macmillan Publishers Limited. All rights reserved

Extended Data Figure 7 | N wave: a novel hippocampal network pattern at 1–4 Hz. a, Non-SWR immobility STAs of wide-band (0.5–400 Hz, upper section) and low frequency-band (1–4 Hz, lower section) filtered LFP. Plotted are mean STAs of hippocampal LFP for each principal unit population (first four columns). LFP from four distinct recording sites (REF, CA2, CA3, DG) are plotted in rows. The mean RTA (fifth column) was calculated from individual RTAs that were matched (same recording epochs) to each CA2 N unit, and thus have the same sample sizes as N units. Vertical lines correspond to the time of spiking (STAs) or SWRs (RTA). The width of the trace indicates ± s.e.m. over individual unit STAs or RTAs. The total trace length is 2 s. REF: reference electrode located in corpus callosum overlying dorsal hippocampus, reporting signals relative to a cerebellar ground screw. Scale bars, *x*, 250 ms; *y*, 50 μV. **b**, All CA2 N unit STAs for spiking during non-SWR immobility. Unit STAs are grouped by polarity at the time of spiking ($t = 0$) and sorted by the time of the extremum (peak for positive; trough for negative) nearest the time of spiking. For each unit, LFP (1–4 Hz) from CA2, CA3, or DG (in increasing order of preference when available) was used. Colours indicate voltage (colour bar). STAs are plotted on the left, while RTAs are plotted on the right. The centre bar indicates the voltage polarity of the STA (orange: positive, black: negative) at the time of spiking (STAs) or SWRs (RTAs), with a dot indicating significance versus 0 μV ($P < 0.05$, rank-sum). The STA of an unclassified unit (see Methods) is indicated with an empty box. **c**, STA versus matched RTA voltage amplitudes (1–4 Hz LFP measured at $t = 0$; STA: *t*ime of spike, RTA: time of peak ripple power) for individual CA2 N units ($n = 58$). CA2 N unit STA amplitudes (black circles) were larger than that of their matched RTAs (pink circles) (mean ± s.e.m., STA: 47 ± 6 μV, RTA: −168 ± 10 μV; $P < 10^{-10}$, signed-rank) and also 0 μV ($P < 10^{-7}$, signed-rank). ***$P < 0.001$. **d**, All interneuronal unit STAs for spiking during non-SWR immobility periods. Interneuronal units were analysed for coupling to LFP since hippocampal interneurons show temporally precise firing relationships with all canonical hippocampal network patterns[80]. Seventy-eight putative interneuronal units were recorded in or near the cell layers of CA1, CA2, CA3, and DG; of these units, 63 were recorded when valid CA2, CA3, or DG LFP recordings were simultaneously available and reporting SWR sharp waves as negative transients. Of the 63 units, 27 fired in association with the N wave (criteria in Methods; CA1: 10, CA2: 4, CA3: 7, and DG: 6). In the plot, unit STAs are grouped by polarity at the time of spiking ($t = 0$) and sorted by the time of the extremum (peak for positive; trough for negative) nearest the time of spiking. For each unit, LFP (1–4 Hz) from CA2, CA3, or DG (in increasing order of preference when available) was used. Colours indicate voltage (colour bar). STAs are plotted on the left, while RTAs are plotted on the right. The centre bar indicates the voltage polarity of the STA (orange: positive, black: negative) at the time of spiking ($t = 0$), with a dot indicating significance versus 0 μV ($P < 0.05$, signed-rank). Unit STAs left unclassified (see Methods) are indicated with an empty box. **e**, Mean firing rate of interneuronal units (mean ± s.e.m.) with negative (black; $n = 36$) versus positive (orange; $n = 27$) STAs. **f**, Firing rate versus speed correlation (Pearson's r) of interneuronal units with negative (black) versus positive (orange) STAs. Task epochs were analysed. **g**, Peri-SWR time histograms (PSTHs) of firing for interneuronal units with negative (left) and positive (right) STAs. Negative STA units uniformly exhibited a sharp peak in firing at the time of SWRs while positive STA units showed instances in which unit firing decreased from baseline levels (unit numbers 1–4, 6 and 8) or showed an increase in firing that was less sharp (unit numbers 23–25)[80–82].

© 2016 Macmillan Publishers Limited. All rights reserved

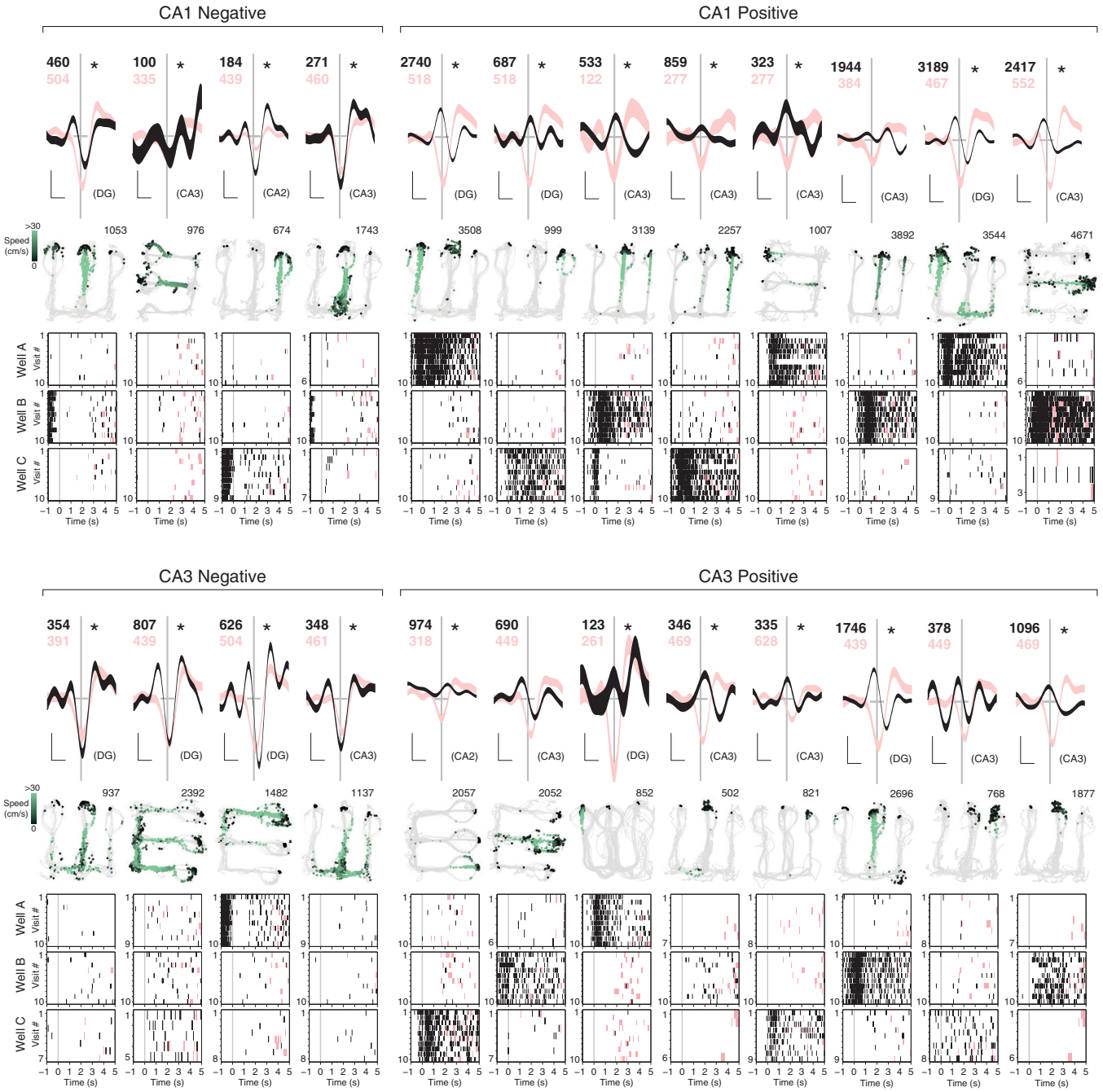


Extended Data Figure 8 | See next page for caption.

© 2016 Macmillan Publishers Limited. All rights reserved

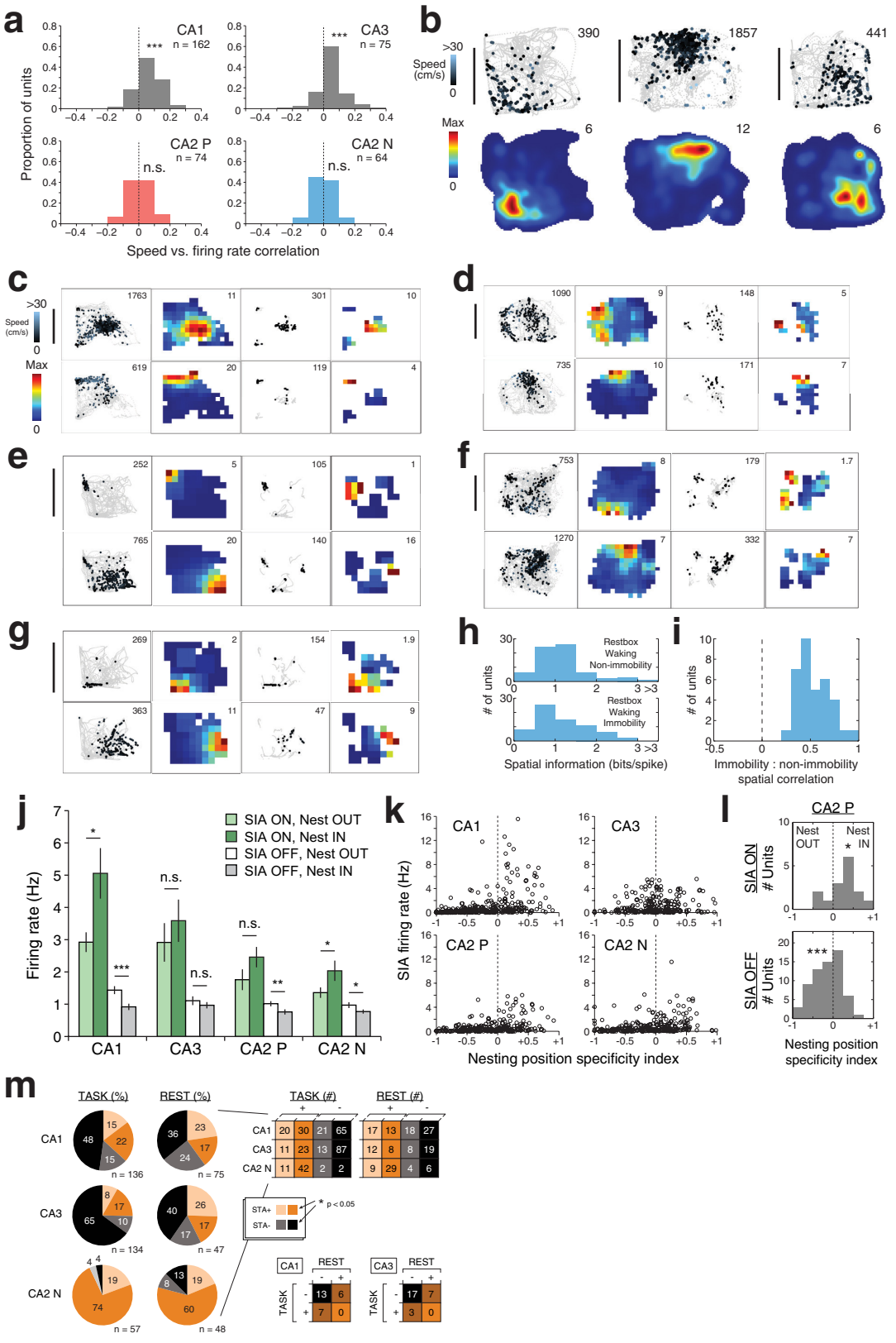
Extended Data Figure 8 | CA1 and CA3 principal neurons fire in association with the N wave. Units showing positive STAs for spiking during non-SWR immobility periods were identified as firing in association with the N wave (N wave-coupled). **a**, All CA1 and CA3 principal unit STAs for spiking during non-SWR immobility periods. Only units with >100 spikes during these periods were analysed. Unit STAs are grouped by polarity at the time of spiking ($t = 0$) and sorted by the time of the extremum (peak for positive; trough for negative) nearest the time of spiking. For each unit, LFP (1–4 Hz) from CA2, CA3, or DG (in increasing order of preference when available) was used. Colours indicate voltage (colour bar at upper right). STAs are plotted on the left, while RTAs are plotted on the right. The centre bar indicates the voltage polarity of the STA (orange: positive, black: negative) at the time of spiking ($t = 0$), with a dot indicating significance versus 0 μV ($P < 0.05$, signed-rank). Unit STAs left unclassified (see Methods) are plotted at bottom and indicated with an empty box. **b**, Firing rates for STA-classified unit populations during task epochs (mean ± s.e.m.; number of units: CA1 negative: 86, CA1 positive: 50, CA3 negative: 100, CA3 positive: 34). In both CA1 and CA3, units with positive STAs showed higher firing rates during non-SWR immobility (CA1 positive versus CA1 negative, $P < 10^{-9}$, rank-sum; CA3 positive versus CA3 negative, $P < 10^{-5}$, rank-sum), similar to CA2 N units (Fig. 2c). **c**, Spatial coverage in CA1 and CA3 units with negative versus positive STAs (mean ± s.e.m.; number of units: CA1 negative: 86, CA1 positive: 50, CA3 negative: 100, CA3 positive: 34). CA1 units with positive STAs showed somewhat lower spatial coverage than units with negative STAs (CA1 negative versus CA1 positive, $P = 0.046$, rank-sum), while an analogous difference in CA3 was not statistically significant (CA3 negative versus CA3 positive, $P = 0.12$, rank-sum). **d**, Well specificity distributions in CA1 and CA3 units that had STA amplitudes (at time of spiking) significantly different from 0 μV (the units marked as significant in **a** and with available well data). For both CA1 and CA3, units with positive STAs showed higher well specificity (mean ± s.e.m., CA1 negative: 0.66 ± 0.04, CA1 positive: 0.86 ± 0.03; CA1 negative versus CA1 positive, $P < 10^{-4}$, rank-sum; CA3 negative: 0.49 ± 0.04, CA3 positive: 0.79 ± 0.04, CA3 negative versus CA3 positive, $P < 10^{-4}$, rank-sum). **e**, Well specificity distributions in CA1 and CA3 units with theta power cutoff. For each task epoch, the distribution of power in the theta band (5–11 Hz), averaged over CA1 recording sites, was calculated for immobility non-SWR periods. Spikes occurring during times in which the theta band power was in the upper quartile of this distribution were then excluded from well specificity calculations. For both CA1 and CA3, units with positive STAs showed higher well specificity (mean ± s.e.m., CA1 negative: 0.73 ± 0.05, CA1 positive: 0.87 ± 0.04; CA1 positive versus CA1 negative, $P < 0.002$, rank-sum; CA3 negative: 0.58 ± 0.04, CA3 positive: 0.80 ± 0.04; CA3 negative versus CA3 positive, $P < 0.004$, rank-sum).

© 2016 Macmillan Publishers Limited. All rights reserved



Extended Data Figure 9 | N wave-coupled CA1 and CA3 principal neurons. Examples of CA1 and CA3 principal units with negative versus positive STAs during non-SWR immobility. Units with positive STAs were defined as N wave-coupled. Each column corresponds to data from an individual unit. Upper sections: non-SWR immobility STA (black trace, ± s.e.m. over individual LFP traces) and RTA (pink trace, ± 2 s.e.m. over individual LFP traces). Vertical lines correspond to the time of spiking (for STAs) or time of SWRs (for RTAs). The total number of spikes (for STAs) and SWRs (for RTAs) averaged is reported at upper left. The region in which the LFP (at 1–4 Hz) was recorded is indicated at lower right. STAs with amplitudes (measured at the time of spiking) significantly different from 0 μV ($P < 0.05$, rank-sum) are marked by an asterisk at upper right. The total trace length is 1 s. A horizontal bar centred at the time of spiking indicates 0 μV and corresponds to 200 ms. Scale bars, *x*, 200 ms; *y*, 50 μV for STA (black trace); 100 μV for RTA (pink trace). Middle sections: spatial firing maps. Positions visited by the subject are plotted in grey while positions at which the unit fired are shown as coloured opaque points (in green) plotted chronologically and with darker colour values at lower speeds. Shown is the 15-min task epoch in which the unit had the highest mean firing rate. The total number of spikes in the epoch is reported at upper right. Spikes occurring during SWR periods are omitted from the plots. Lower sections: well firing rasters. The time of well entry ($t = 0$) is plotted as a grey line. SWR periods are plotted in the background as pink zones.

© 2016 Macmillan Publishers Limited. All rights reserved



Extended Data Figure 10 | See next page for caption.

© 2016 Macmillan Publishers Limited. All rights reserved

Extended Data Figure 10 | Hippocampal spatial coding in the rest environment. a, Distribution of correlations (Pearson's *r*) between firing rate and log speed for each unit population in awake periods in the rest environment. Mean ± s.d.; CA1 ($n = 162$ units): 0.06 ± 0.07, CA1 versus 0, $P < 10^{-17}$, signed-rank; CA3 ($n = 75$): 0.05 ± 0.08, CA3 versus 0, $P < 10^{-6}$, signed-rank; CA2 P ($n = 74$): 0.01 ± 0.07, CA2 P versus 0, $P = 0.55$, signed-rank; CA2 N ($n = 64$): 0.00 ± 0.07, CA2 N versus 0, $P = 0.77$, signed-rank, CA2 N versus CA2 P, $P = 0.47$. Only units with significant correlations ($P < 0.05$) were included (CA1: 162/163 units, CA3: 75/76, CA2 P: 74/76 units, CA2 N: 64/68 units). The N unit population did not show a significant relationship between firing rate and speed, unlike in the task environment (Fig. 2b). The positive correlation between firing rates and speed was also absent in the CA2 P population, suggesting a broader weakening of speed-dependent changes in hippocampal firing in the rest environment. This could be due to the restricted range of speeds in the rest environment enclosure and/or a fundamental influence of task conditions (Extended Data Fig. 1) on hippocampal neural activity. **b**, Three additional example N unit spatial firing maps in the rest environment. Plotted are data from awake periods. Each column corresponds to data from an individual unit. Upper row: raw maps showing positions visited by the subject (grey) and positions where the unit fired (coloured opaque points, plotted chronologically and with darker colour values at lower speeds). Total number of spikes (outside of SWR periods) in the epoch is reported at upper right. Lower row: occupancy-normalized firing maps. Peak spatial firing rate is reported at upper right. Scale bar, 20 cm. **c–g**, Awake immobility spatial firing in five example co-recorded pairs of N units from single rest recording epochs. The example pair in **c** is the same as shown at bottom in Fig. 5d. For each example pair, a unit corresponds to a row. The leftmost two columns (raw and occupancy-normalized firing maps) correspond to data from awake periods, while the rightmost two columns (raw and occupancy-normalized firing maps) correspond to data from awake immobility periods. Reported at upper right are total spike counts (raw maps) or peak spatial rates (occupancy-normalized maps). Bin size: 2.5 cm. Scale bar: 20 cm. Here, the occupancy-normalized maps shown were generated from unsmoothed occupancy-normalized maps by taking the mean firing rate of bins of a 3×3 grid centred on the bin, disregarding bins that were not occupied by the subject. Quantification in **h** and **i** was performed on unsmoothed occupancy-normalized maps. **h**, Spatial information[83] of N units in awake periods outside of immobility periods (upper plot, 1.12 ± 0.59 bits per spike, $n = 67$ units, with one unit excluded due to lack of firing outside of immobility) and awake immobility periods (lower plot, 1.17 ± 0.58 bits per spike, $n = 68$ units). In both conditions, data during SWR periods were excluded. Spatial information was calculated in the rest epoch in which the unit had the highest mean firing rate during awake periods. As in the task environment, N units exhibited spatially specific firing during immobility. Notably, the rest environment is an additional condition in which N units signalled location, moreover in the absence of material reward (analysis of non-reward locations in the task maze in Extended Data Fig. 5b–d). **i**, Correlation (Pearson's *r*) of N unit spatial maps between awake immobility periods and awake non-immobility periods in the rest environment. The correlation was calculated from unsmoothed occupancy-normalized firing maps, specifically for spatial bins in which the subject was immobile. Out of 67 units, 35 showed significant correlation ($P < 0.05$; 0.53 ± 0.03, mean ± s.e.m.), with no negative correlations observed. Correlations were calculated in the rest epoch in which the unit had the highest mean firing rate during awake periods. These positive correlations indicate that N units retained their spatial specificity into immobility periods. **j**, Comparison of firing rates across SIA-nesting conditions. Statistical tests (signed-rank, comparison of Nest OUT versus IN): CA1, SIA ON ($n = 18$ units), $P = 0.014$; CA1, SIA OFF ($n = 92$), $P < 10^{-5}$; CA3, SIA ON ($n = 19$), $P = 0.60$; CA3, SIA OFF ($n = 58$), $P = 0.26$; CA2 P, SIA ON ($n = 15$), $P = 0.11$; CA2 P, SIA OFF ($n = 65$), $P = 0.0027$; CA2 N, SIA ON ($n = 18$), $P = 0.022$; CA2 N, SIA OFF ($n = 57$), $P = 0.027$. As in the evaluation of the nesting position specificity index (Fig. 5f), these comparisons show that the CA1 and CA2 N unit populations met dual criteria (description in Methods) for nesting position coding, while the CA3 unit population did not. $^{*}P < 0.05$; $^{**}P < 0.01$; $^{***}P < 0.001$; n.s., not significant at $P < 0.05$. **k**, SIA firing rate versus nesting position specificity index for all detected unit-sleep period samples. Here, if data was available for a unit (in the rest unit set) during a detected sleep period, then the unit's SIA firing rate during the sleep period was measured and its nesting position specificity index was calculated with respect to that sleep period's nesting position; this sample is then represented by a scatter point. In this approach, an individual unit can contribute more than one sample. CA1 ($n = 312$ samples from 94 units): Spearman's ρ: 0.55, $P < 10^{-25}$. CA3 ($n = 223$ samples from 62 units): Spearman's ρ: 0.12, $P = 0.065$. CA2 P ($n = 263$ samples from 65 units): Spearman's ρ: 0.37, $P < 10^{-9}$. CA2 N ($n = 256$ samples from 60 units): Spearman's ρ: 0.33, $P < 10^{-7}$. **l**, CA2 P unit distribution of nesting position specificity indices. Mean ± s.e.m.: SIA ON ($n = 15$): 0.22 ± 0.09, $P = 0.048$, signed-rank; SIA OFF ($n = 65$): -0.16 ± 0.04, $P < 0.001$, signed-rank. $^{*}P < 0.05$; $^{***}P < 0.001$. **m**, STA class proportions across conditions. In addition to STAs calculated from non-SWR immobility in task epochs (TASK, presented in Fig. 4 and Extended Data Figs 7, 8 and 9), STAs were also calculated from non-SWR immobility during awake periods in rest epochs (REST). For REST STAs, as in TASK STAs, a minimum of 100 spikes outside of SWR periods during awake immobility and valid LFP reference sites were required, and units with STAs with mixed features were left unclassified (LFP reference site and unclassified STA criteria in Methods; unclassified unit counts: CA1: 8 out of 83, CA3: 4 out of 51, CA2 N: 10 out of 58). As in TASK, N wave-coupled units in REST were detected in substantial proportions. In left and upper right diagrams, STA positive (N wave-coupled) is in light orange, with a darker orange corresponding to significance in the STA voltage at $t = 0$ ($P < 0.05$, signed-rank). STA negative is in grey, with black corresponding to significance. Left (pie charts): proportions (%) of units in each of the STA classes. Total unit counts (number of units with classified STAs) are reported at bottom right. Percentages are rounded to nearest whole number. Upper right: unit counts in each (non-overlapping) category. Lower right: contingency table for CA1 and CA3 units found active in both task and rest epochs (fired >100 spikes outside of SWR periods during immobility in at least one task recording epoch and during awake immobility in at least one rest recording epoch) and with classifiable STAs (positive versus negative). Notably, no units were observed that were STA positive in both conditions, suggesting that N wave-coupling for a given CA1/CA3 neuron is not a static property. In contrast, the majority of classifiable CA2 N units in both TASK (53/57, or 93%) and REST (38/48, or 79%) were N wave-coupled.

© 2016 Macmillan Publishers Limited. All rights reserved